Jordanian Journal of Computers and Information Technology

August 2018 | VOLUME 04 | NUMBER 02 | ISSN 2415 - 1076 (Online) ISSN 2413 - 9351 (Print)

JJCIT

www.jjcit.org jjcit@psut.edu.jo

An International Peer-Reviewed Scientific Journal
Financed by the Scientific Research Support Fund

Jordanian Journal of Computers and Information Technology (JJCIT)

The Jordanian Journal of Computers and Information Technology (JJCIT) is an international journal that publishes original, high-quality and cutting edge research papers on all aspects and technologies in ICT fields.

JJCIT is hosted by Princess Sumaya University for Technology (PSUT) and supported by the Scientific Research Support Fund in Jordan. Researchers have the right to read, print, distribute, search, download, copy or link to the full text of articles. JJCIT permits reproduction as long as the source is acknowledged.

AIMS AND SCOPE

The JJCIT aims to publish the most current developments in the form of original articles as well as review articles in all areas of Telecommunications, Computer Engineering and Information Technology and make them available to researchers worldwide. The JJCIT focuses on topics including, but not limited to: Computer Engineering & Communication Networks, Computer Science & Information Systems and Information Technology and Applications.

INDEXING

JJCIT is indexed in:

- DOAJ
  https://doaj.org
- CrossRef
  http://search.crossref.org/?q=jjcit
- OCLC WorldCat
  http://www.worldcat.org/search?qt=worldcat_org_all&q=jjcit
- Scilit
  http://www.scilit.net/journals/387088
- BASE - Bielefeld Academic Search Engine
  https://www.base-search.net/Search/Results?lookfor=jjcit&name=&oaboost=1&newsearch=1&refid=dcbasen
- Google Scholar
  https://scholar.google.com/citations?user=88ospLoAAAAJ&hl=en

Jordanian Journal of Computers and Information Technology (JJCIT), Vol. 04, No. 02, August 2018.

MOTOR IMAGERY EEG SIGNAL PROCESSING AND CLASSIFICATION USING MACHINE LEARNING APPROACH

S. R. Sreeja[1], Debasis Samanta[1], Pabitra Mitra[1] and Monalisa Sarma[2]

(Received: 6-Dec.-2017, Revised: 5-Mar.-2018, Accepted: 10-Mar.-2018)

ABSTRACT

Typically, people with severe motor disabilities have limited opportunities to socialize. Brain-Computer Interfaces (BCIs) can be seen as a hope of restoring freedom to immobilized individuals. Motor imagery (MI) signals recorded via electroencephalograms (EEGs) are the most convenient basis for designing BCIs as they provide a high degree of freedom. MI-based BCIs help motor disabled people to interact with any real-time BCI applications by performing a sequence of MI tasks. But, inter-subject variability, extracting user-specific features and increasing accuracy of the classifier are still a challenging task in MI-based BCIs. In this work, we propose an approach to overcome the above-mentioned issues. The proposed approach considers channel selection, band-pass filter based common spatial pattern, feature extraction, feature selection and modeling using Gaussian Naïve Bayes (GNB) classifier. Since the optimal features are selected by feature selection techniques, they help overcome inter-subject variability and improve performance of GNB classifier. To the best of our knowledge, the proposed methodology has not been used for MI-based BCI applications. The proposed approach has been validated using BCI competition III dataset IVa. The result of our approach has been compared with those of two classifiers; namely, Linear Discriminant Analysis (LDA) and Support Vector Machine (SVM). The results prove that the proposed method provides an improved accuracy over LDA and SVM classifiers. The proposed method can be further developed to design reliable and real-time MI-based BCI applications.

KEYWORDS

Motor imagery, Brain computer interface, Electroencephalography, Feature extraction, Feature selection, Machine learning.

1. INTRODUCTION

Brain-Computer Interfaces (BCIs) provide a direct connection between the human brain and a computer [1]. BCIs capture neural activities associated with external stimuli or mental tasks, without any involvement of nerves and muscles and provide an alternative non-muscular communication [2]. The interpreted brain activities are directly translated into a sequence of commands to carry out specific tasks, such as controlling wheel chairs, home appliances, robotic arms, speech synthesizers, computers and gaming applications. Brain activities can be measured through invasive and non-invasive devices. So far, a wide research has been carried out on human behaviour and task classification using invasive techniques, such as electrocorticography (ECoG) [3] and Local Field Potentials (LFPs) [4]-[5]. In ECoG, the electrodes are placed directly on the exposed surface of the brain to record electrical activity and LFP refers to the electrical field recorded using a small-sized electrode in the extracellular space of brain tissue. These techniques involve surgery and are risky. A non-invasive BCI uses brain activities recorded from an electroencephalogram (EEG), functional Magnetic Response Image (fMRI) or magnetoencephalogram (MEG), …etc. Among the available non-invasive devices, EEG-based BCIs facilitate many real-time applications, as they satisfy convenience criteria (non-intrusive, non-obtrusive and simple) and effectiveness criteria (sensitive, efficient and compatible) [6].

This paper is an extended version of a short paper that was presented at the International Conference "New Trends in Computing Sciences (ICTCS) 2017", 11-13 October 2017, Amman, Jordan.

1. S. R. Sreeja, Debasis Samanta and Pabitra Mitra are with Department of Computer Science and Engineering, Indian Institute of Technology Kharagpur, West Bengal, India. Emails: sreejasr@iitkgp.ac.in, dsamanta@iitkgp.ac.in, pabitra@cse.iitkgp.ernet.in.
2. Monalisa Sarma is with Subir Chowdhury School of Quality and Reliability, Indian Institute of Technology Kharagpur, West Bengal, India. Email: monalisa@iitkgp.ac.in.

EEG-based BCI systems are mostly built using Visually Evoked Potentials (VEPs), Event-Related Potentials (ERPs) [7], Slow Cortical Potentials (SCPs) and Sensori-Motor Rhythms (SMRs). Out of these potentials, SMR-based BCI provides a high degree of freedom in association with real and imaginary movements of hands, arms, feet and tongue [8]. The neural activities associated with SMR-based motor imagery (MI) BCI are the so-called mu (7-13 Hz) and beta (13-30 Hz) rhythms [9]. These rhythms are readily measurable in both healthy and disabled people with neuromuscular injuries. Upon executing real or imaginary motor movements, amplitude suppression or enhancement of μ rhythm is caused and these phenomena are called Event-Related Desynchronization (ERD) and Event-Related Synchronization (ERS), respectively [9]. Traditional BCIs rely on these neurophysiological phenomena to determine whether the user is performing a motor task or not.

As the dynamics of brain potentials associated with MI tasks can form spatio-temporal patterns, the Common Spatial Pattern (CSP) [10] is a highly successful algorithm to extract relevant MI features. This algorithm is designed to capture the spatial projections of ERD/ERS in such a way that the power ratio differs greatly between two classes. Several variants of CSP have been devised, such as Common Spatial Spectral Pattern (CSSP) [11], spectrally weighted common spatial pattern [12], Iterative Spatio-Spectral Pattern Learning (ISSPL) [13], Filter Bank Common Spatial Pattern (FBCSP) [14], augmented complex common spatial pattern [15], Separable Common Spatio-Spectral Pattern (SCSSP) [16] and self-adaptive CSP [17].

Collecting EEG-based MI data is a tedious and time-consuming process. Processing with entire EEG data delays the system and affects the accuracy of the classifier. It is also important to note that, for the same user, the observed patterns differ from one day to another, or from session to session [1]. This inter-personal variability of EEG signals results in degraded performance of the classifier. From the literature, it is observed that many features, like statistical [18], time-domain [19], frequency-domain [20], wavelet [21], auto-regressive coefficients [22] have been extracted from MI-based EEG signals. It is still a question whether the extracted features are subject-specific optimal features or not. Apart from this issue, for real-time applications, the ongoing motor imagery events have to be detected and classified continuously into a control command as accurately and quickly as possible. The above issues motivate us to lay down our research objectives as follows: selecting channels considering the motor areas; addressing inter-personal variability; extracting the set of highly discriminant user-specific features; increasing the speed and accuracy of the classifier in MI-based BCI system.

As it is proven that the channels present near the active regions of the brain have more relevant information [18], it is best to consider those channels for further processing. Few research on feature optimization for MI-based BCI [23] and Steady-State VEP (SSVEP)-based BCI [24] has been carried out recently. In this work, to provide subject-specific optimal features, two different feature selection methodologies, such as minimum Redundancy Maximum Relevancy (mRMR) method and Lasso regularization-based feature selection method are studied. In the same way, in literature, different classifiers have been applied to classify EEG-based MI tasks with different features [25]. Recent research on classification and pattern recognition shows that a Bayesian classifier produces enhanced results than the existing classifiers [26]– [29]. Hence, in this work, Gaussian Naïve Bayes (GNB) classifier is used and modeled using the selected optimal features.

The framework of the proposed EEG-based MI BCI system is shown in Figure 1. The following aspects can be highlighted on the proposed EEG-based MI BCI system.

1) The channels present over the motor areas are selected for processing.

2) Band-pass filter-based CSP is applied to the selected EEG channels to spatially filter the signals.

3) The possible number of features is extracted from the spatially filtered data.

4) The most discriminant user-specific features using two different feature selection methods are observed.

5) The selected features are modeled using Gaussian Naïve Bayes classifier.

6) We compared the experimental results of the proposed method with those of two classifiers; namely, LDA and SVM, in terms of accuracy and time.

In order to make our proposed method more suitable for real-time classification, constraints are

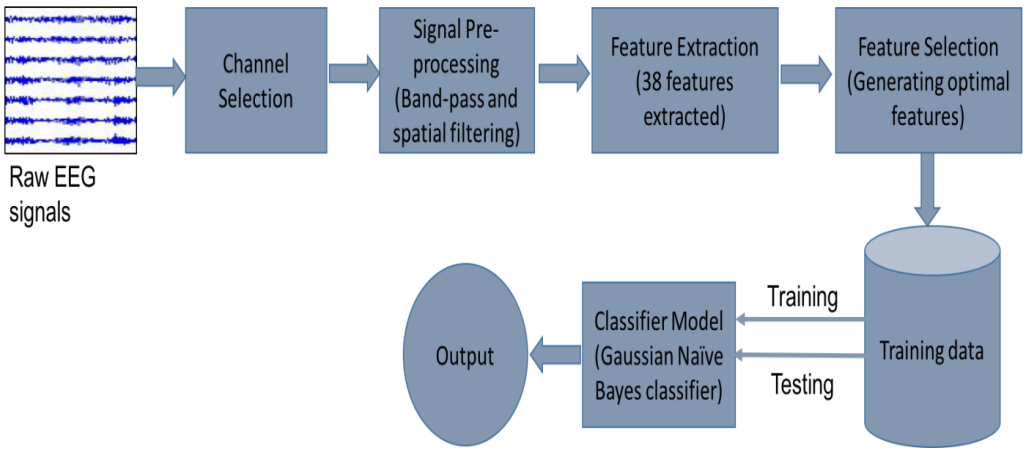

Figure 1. Framework of the proposed approach.

applied on selecting channels and on selecting features. Normally, EEG signals suffer from inter-and intra-subject variability. In our proposed method, the selected features are normalized using z-score normalization, which makes the features lie in a certain range and reduces the variability between different sessions and subjects. Unlike other classifiers, in GNB classifier, there is no parameter tuning. Finally, only with two feature sets, the GNB classifier classifies the different MI tasks accurately and quickly. The pipeline followed in our work, like channel selection, band-pass filter-based CSP, feature selection and GNB model, proves to be a better method for real-time MI-based BCI applications.

Our paper is organized as follows. In Section 2, we present a description of the data and the proposed technique in detail. In Section 3, the experimental results and performance evaluation are presented. Finally, conclusions and future work are outlined in Section 4.

2. DATA AND METHOD

This section will describe the MI data used in this research and then the steps followed in the proposed method; namely, channel selection, pre-processing, feature extraction, feature selection and classification of EEG-based MI data in detail.

2.1 Experimental Data

We used the publicly available dataset IVa from BCI competition III [30] to validate the proposed approach. The dataset consists of EEG-recorded data from five healthy subjects (aa, al, av, aw and ay), who performed right hand and right foot MI tasks during each trial. According to the international 10-20 system, MI signals were recorded from 118 channels. The visual cue for 1 trial lasted for 3.5 seconds and the time paradigm of a single trial is shown in Figure 2. For each subject, there were 140

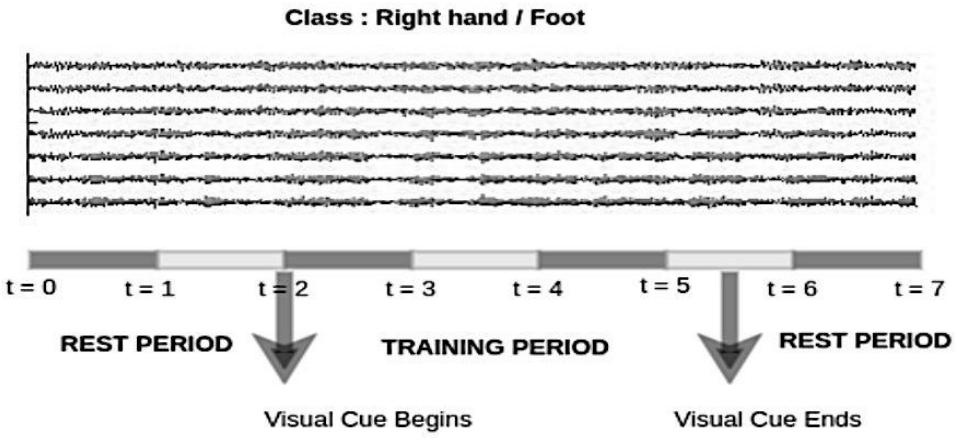

Figure 2. Time taken for a single trial.

trials for each task and therefore 280 trials totally. The measured EEG signal was filtered using a bandpass filter between 0.05 and 200 Hz. Then the signal was digitized at 1000 Hz with 16-bit accuracy.

2.2 EEG Signal Pre-processing

2.2.1 Channel Selection

The dataset consists of EEG recordings from 118 channels, which means that it is very large to process. As we are using the EEG signal of two class MI tasks (right-hand and right-foot), we extract the needed information from premotor cortex, supplementary motor cortex and primary motor cortex [31]. Therefore, from the 118 channels of EEG recording, 30 channels present over the motor cortex are considered for further processing. Moreover, removal of irrelevant channels helps increase the robustness of classification system [32]. The selected channels are FC2, FC4, FC6, CFC2, CFC4, CFC6, C2, C4, C6, CCP2, CCP4, CCP6, CP2, CP4, CP6, FC5, FC3, FC1, CFC5, CFC3, CFC1, C5, C3, C1, CCP5, CCP3, CCP1, CP5, CP3 and CP1. The motor cortex and the areas of motor functions, the standard 10±20 system of electrode placement of 128-channel EEG system and the electrodes selected for processing shown in Figure 3. The green and red circle indicates the selected channels and the red circle indicates the C3 and C4 channels on the left and right side of the scalp, respectively.

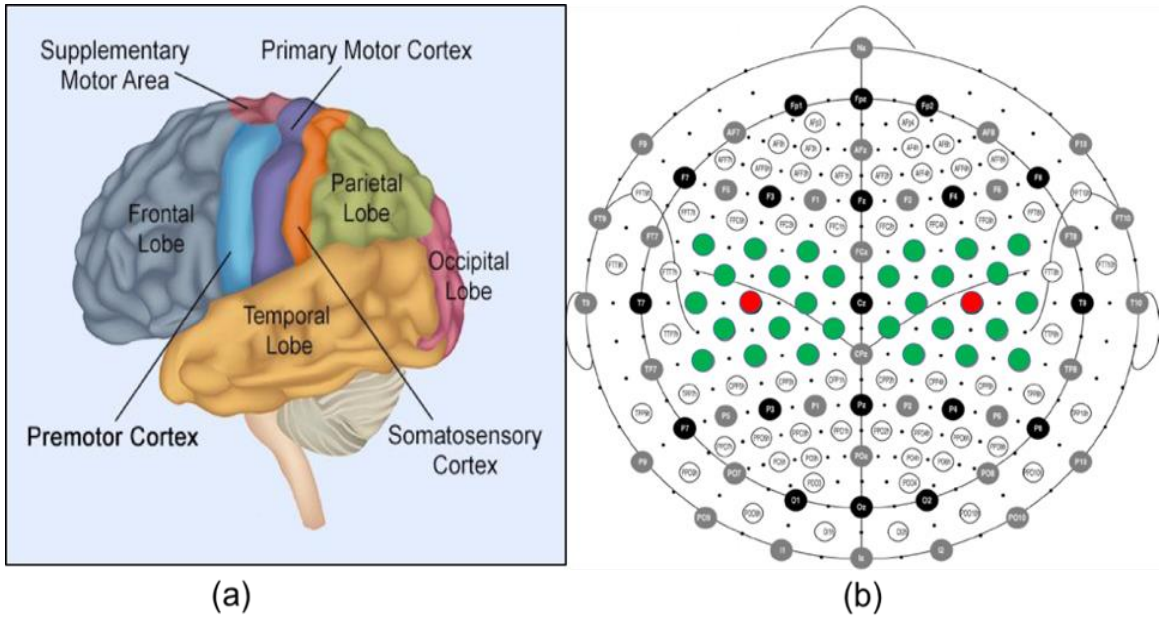

Figure 3. (a) Motor cortex of the brain (b) Standard 10±20 system of electrode placement for 128-channel EEG system. The electrodes in green and red color are selected for processing.

2.2.2 Bandpass Filtering

Since the original sampling rate of the EEG signal is 1000 Hz, it is down sampled to 100 Hz for further processing. Then, the selected 30-channel EEG data is again passed through a band-pass filter between 7 and 30 Hz, as it is known from [9] that mu (μ) and beta (β) rhythms lie within that frequency range. Then, data segmentation is done, where we used three-second data (300 samples) after the display of cue of each trial, assuming that the subject might be moving the right hand or right foot on an average of 3 seconds. Each segmented data is called an epoch.

2.2.3 Spatial Filtering

CSP is one of the most commonly used spatial filters in building MI-based BCIs [10]–[17]. The signals which are segmented into two second time samples are spatially filtered using a CSP filter. CSP aims to find the linear transforms or spatial filters, which maximizes the variance of one class while minimizing it for the other class. How CSP is applied to the given dataset, is explained here.

Jordanian Journal of Computers and Information Technology (JJCIT), Vol. 04, No. 02, August 2018.

Let $\boldsymbol{X}_H$ and $\boldsymbol{X}_F$ be the two epochs of a multivariate signal related to right-hand and right-foot MI classes, respectively. They are both of size ($c \times n$), where c is the number of channels (30) and n is the number of samples (100×2). We denote the CSP filter by:

$$\boldsymbol{X}_i^{\boldsymbol{CSP}} = \boldsymbol{W}^{\boldsymbol{T}}\boldsymbol{X}_{\boldsymbol{i}} \tag{1}$$

where $i \in \{H, F\}$ is the number of MI classes, $\boldsymbol{X}_i^{\boldsymbol{CSP}}$ is the spatially filtered signal, W is the spatial filter matrix and $\boldsymbol{X}_{\boldsymbol{i}} \in \mathbb{R}^{c \times n}$ is the input signal to the spatial filter. The objective of the CSP algorithm is to estimate the filter matrix $\boldsymbol{W}$. This can be achieved by finding the vector w, the component of the spatial filter $\boldsymbol{W}$, by satisfying the following optimization problem:

$$\max_{w}\left(\frac{w^T C_H w}{w^T C_F w}\right) \tag{2}$$

where $C_H = \boldsymbol{X}_H\boldsymbol{X}_H^T$ and $C_F = \boldsymbol{X}_F\boldsymbol{X}_F^T$. In order to make the computation easier to find w, we computed $\boldsymbol{X}_H$ and $\boldsymbol{X}_F$ by taking the average of all epochs of each class. Equation (2) can be written as minimization problem as follows:

$$\min_{w}(-w^T C_H w) \quad \text{Subject to} \quad w^T C_F w = 1 \tag{3}$$

Solving the above equation using Lagrangian method, we finally have the resulting equation as:

$$C_H w = \lambda C_F w \tag{4}$$

Thus, Equation (2) becomes an eigenvalue decomposition problem, where λ is the eigenvalue which corresponds to the eigenvector w, obtained by solving the following equation:

$$(C_H - \lambda C_F)w = 0 \tag{5}$$

Here, w maximizes the variance of right-hand class, while minimizing the variance of right-foot class. The eigenvectors with the largest eigenvalues for C_H have the smallest eigenvalues for C_F. Since we used 30 EEG channels, we will have 30 eigenvalues and correspondingly 30 eigenvectors. Therefore, CSP spatial filter $\boldsymbol{W}$ will have 30 column vectors. From that, we select the first m and last m columns to use as $2m$ CSP filter of $\boldsymbol{W}_{CSP}$.

$$\boldsymbol{W}_{CSP} = [w_1, w_2, \dots, w_m, w_{c-m+1}, \dots, w_c] \in \mathbb{R}^{2m \times c} \tag{6}$$

Therefore, for the given two-class epochs of MI data, the CSP filtered signals are defined as follows:

$$\boldsymbol{X}_H^{CSP} \in \mathbb{R}^{2m \times c} \coloneqq \boldsymbol{W}_{CSP}^T\boldsymbol{X}_H$$

$$\boldsymbol{X}_F^{CSP} \in \mathbb{R}^{2m \times c} \coloneqq \boldsymbol{W}_{CSP}^T\boldsymbol{X}_F \tag{7}$$

The CSP filters can be plotted back to see the activations of various regions of the brain. Figure 4 shows the scalp plot, where the first 4 and last 4 magnitudes of the coefficients of the CSP filter are plotted. The dark red colour indicates the highest significance. The upper-left plot indicates the filter w_1 and the down-right plot indicates the last filter w_n.

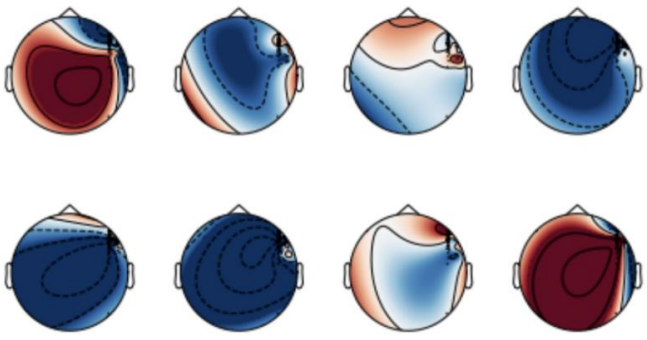

Figure 4. Colormap of magnitudes of the coefficients of CSP filter projected on the scalp.

2.3 Feature Extraction

The spatially filtered signals $\boldsymbol{X}_i^{CSP}$ are obtained for each epoch and are still of high dimension. To reduce the complexity of working with such high dimensional signals, we need to pull out some special features from the spatially filtered data. These features must maximize the discriminability

between the two MI classes. A set of 38 features are extracted from each spatially filtered epoch. The extracted feature vectors are listed below.

2.3.1 Statistical Features

We extracted seven statistical features; namely, mean, median, standard deviation, skewness, kurtosis, maximum and minimum, as stated in Table 1. These features describe the distribution of EEG signals in terms of amplitudes and moments [18].

Table 1. Statistical features and their description.

Parameters	Description
Mean	Mean value of the signal, $\mu_{X_i^{CSP}} = \frac{1}{N}\sum_{k=0}^{N-1} x_k$
Median	Median (middle) value of the signal
Standard deviation	Standard deviation of the signal, $\sigma_{X_i^{CSP}} = \sqrt{\frac{1}{N-1}\sum_{k=0}^{N-1}(x_k - \mu_{X_i^{CSP}})^2}$
Skewness	Asymmetry value of the signal, $S_{X_i^{CSP}} = \frac{\frac{1}{N}\sum_{k=0}^{N-1}(x_k - \mu_{X_i^{CSP}})^3}{\sigma_{X_i^{CSP}}{}^3}$
Kurtosis	Flatness measure of the signal, $K_{X_i^{CSP}} = \frac{\frac{1}{N}\sum_{k=0}^{N-1}(x_k - \mu_{X_i^{CSP}})^4}{(\sigma_{X_i^{CSP}}{}^2)^2} - 3$
Maximum	Maximum positive amplitude
Minimum	Minimum negative amplitude

2.3.2 Time-domain Features

Time-domain features [19] capture the temporal information of signals. As EEG is known to have a good temporal locality, we extracted a number of time-domain features, as listed in Table 2; namely, hjorth parameters (activity, mobility and complexity), 1st difference mean and maximum, 2nd difference mean and maximum, mean and variance of vertex to vertex slope, mean and variance of vertex to vertex amplitudes, zero crossing and coefficient of variation.

Table 2. Time-domain features and their description.

Parameters	Description
Activity	Mean power/variance ($\sigma^2_{X_i^{CSP}}$)
Mobility	$\left(\frac{\sigma'_{X_i^{CSP}}}{\sigma_{X_i^{CSP}}}\right)$, where $\sigma'_{X_i^{CSP}}$ is the standard deviation of first derivative
Complexity	$\left(\frac{\sigma''_{X_i^{CSP}}}{\sigma'_{X_i^{CSP}}} / \frac{\sigma'_{X_i^{CSP}}}{\sigma_{X_i^{CSP}}}\right)$, where $\sigma''_{X_i^{CSP}}$ is the stand. devi. of second derivative
1st Diff. Mean and Max.	Mean and maximum value of the first derivative of the signal
2nd Diff. Mean and Max.	Mean and maximum value of the second derivative of the signal
Mean V-V slope	Mean of vertex to vertex (peak-peak) slope
Variance V-V slope	Variance of vertex to vertex (peak-peak) slope
Mean V-V amplitudes	Mean of vertex to vertex (peak-peak) amplitudes
Variance V-V amplitudes	Variance of vertex to vertex (peak-peak) amplitudes
Zero crossing	Number of times the signal crossing zero
Coeff. of variation	Ratio of standard deviation to the mean.

2.3.3 Frequency-domain features

The frequency-domain features [20] capture the frequency information of brain rhythms during motor imagery tasks. It is known as stated earlier that the frequency of motor imagery signals lies within 7-30 Hz. If the time-domain signal is converted into frequency domain, all frequency related features can be estimated. Power spectral density (PSD) is used to estimate the frequency content of the signal. In our work, PSD is computed using Welch method, where averaging a periodogram spectrum is carried out on overlapping data segments. The spatially filtered signal (300 samples) is divided into small segments and assumed to be stationary. A window function, such as rectangular, hamming, hanning, …etc., is typically chosen for this purpose. For computing PSD, we used Hanning window and took the window size as 100 with 50% overlapping. From the obtained array of frequencies, we selected two sub-bands of α (7-13 Hz) and β (13-30 Hz). For each of these sub-bands, we calculated the band power and its ratios (α/β and β/α). PSD obtained for the given spatially filtered signal is shown in Figure 5.

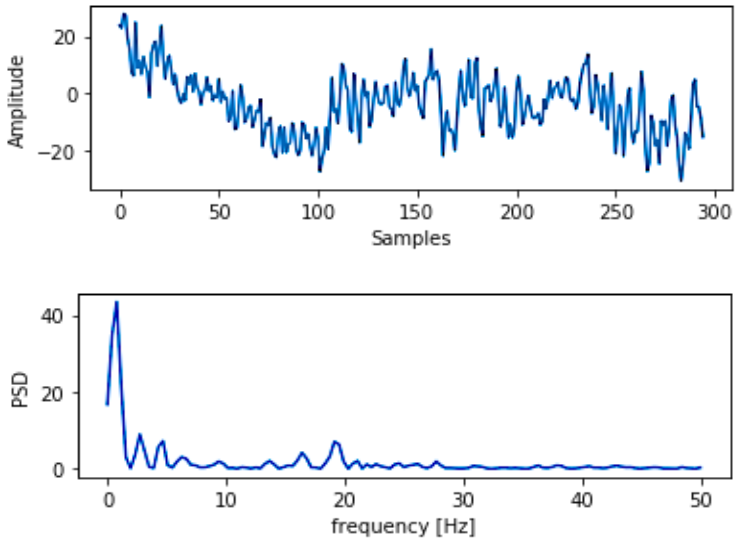

Figure 5. Spatially filtered signal of an epoch and its PSD.

2.3.4 Wavelet-based Features

Wavelet transform [21] is a spectral estimation technique, in which any general function can be expressed as an infinite series of wavelets. The decomposition of the signal leads to a set of coefficients called wavelet coefficients. In our work, we used the Discrete Wavelet Transform (DWT), which employs two functions; namely, scaling function and wavelet function. The DWT gives rise to two coefficients (D_i and A_i), which are the down sampled outputs of the high pass and low pass filters at each decomposition level. Features may be computed for any D_i and A_i corresponding to important MI-based EEG frequency bands. We used *coif1* wavelet with level-1 decomposition, as it gives best result among other wavelets [33]. Here, D_i corresponds to beta-band (13-30 Hz) and A_i corresponds to alpha-band (7-13 Hz). The extracted wavelet-based features are mean, standard deviation, energy and entropy of both D_i and A_i.

2.3.5 Auto-regressive Coefficients

Auto-regressive (AR) method [22] models the signal at any given time, as a weighted sum of signals at previous time and some noise. We implemented AR model of order 6 using the Burg's algorithm and used the coefficients as features. Mathematically, it can be formulated as:

$$X(t) = a_1 X(t_1) + a_2 X(t_2) + \cdots + a_p X(t_p) + E_t \quad (8)$$

where, $X(t)$ is the measured signal at time t, E_t is the noise term and a_1 to a_p are the auto-regressive parameters.

Therefore, we extracted a set of N (38) features from each spatially filtered epoch; i.e., $F = \{f_1, f_2, \dots, f_N\}$, where $f_1 \in \mathbb{R}^{2k}$ and $F \in \mathbb{R}^{2k \times N}$.

2.3.6 Feature Normalization

The extracted feature vectors are then normalized to a common range to reduce inter-and intra-subject variability. We used z-score normalization [34], so that the mean value of the signal is zero and the standard deviation is one. Mathematically, this is defined as:

$$z = \frac{x-\mu}{\sigma} \tag{9}$$

where μ is the mean and σ is the standard deviation. Then, out of these normalized features, the discriminative subset of features has to be identified for a reliable classification.

2.4 Feature Selection

Feature selection approaches aim to select a small set of features S with dimension m; that is, $S = \{s_1, s_2, \dots, s_m\}$ from a feature set $F = \{f_1, f_2, \dots, f_N\}$, where $m \leq N$ and $S \subseteq F$. Reducing the number of irrelevant features will drastically improve the learning performance, lower the computational complexity and decrease the required storage. In this section, we have exercised two feature selection algorithms over the above normalized feature vectors.

2.4.1 Minimum-redundancy and maximum-relevance (mRMR)

As the name suggests, this feature selection algorithm is based on selecting features with minimum redundancy and maximum relevance depending on the mutual information values between various features [35]. Thus, it involves selecting the feature S with the highest relevance to the target class C, based on mutual information, such that $I(S;C)$. Mathematically, this is defined as:

Maximum relevance:

$$\max D, \qquad D = \frac{1}{|S|}\sum_{f_i \in S} I(f_i; C) \tag{10}$$

Minimum redundancy:

$$\min R, \qquad R = \frac{1}{|S|^2}\sum_{f_i, f_j \in S} I(f_i; f_j) \tag{11}$$

where $I(f_i; f_j)$ is mutual information between the feature f_i and f_j, $|S|$ is the cardinality of the set S and C is the target class. The criterion of combining the above two constraints is called minimum-redundancy maximum-relevancy (mRMR) and is given as:

$$\max \Phi, \qquad \Phi = D - R \tag{12}$$

The features are sorted according to mRMR and the first three features are selected as optimal features. The selected features are given in Table 1.

2.4.2 Lasso Regularization-based Feature Selection

In regularization models, classifier induction and feature selection are simultaneously achieved by minimizing fitting errors and properly tuning penalties. The learned classifier w can have coefficients to be very small or zero. Feature selection is achieved by selecting the non-zero coefficients in w [36]. Mathematically, this is defined as:

$$\hat{w} = \min_{w} c(w, X) + \alpha\|w\| \tag{13}$$

where $c(w, X)$ is the objective function of the classifier, α is the regularization parameter and $\|w\|$ is a regularization (penalty) term. The model penalized with l_1 norm is called Lasso regularization and is defined as:

$$\|w\| = \sum_{i=1}^{m} w_i \tag{14}$$

This model will have a sparse solution, such that it forces weak features to have zero coefficients and be excluded from the model. Thus, Lasso (l_1) regularization inherently performs feature selection [37].

The selected features are listed in Table 3.

Table 3. Feature selection methods and the selected optimal features.

Feature Selection Method	Selected Features
Minimum-redundancy Maximum-relevancy (mRMR)	Band-power (13-30 Hz), wavelet energy of D_i, kurtosis
Lasso Regularization	Band-power (13-30 Hz), wavelet energy of D_i, AR with 6 coefficients

In both feature selection methods, we selected three features as mentioned in Table 3. Then, the common features between mRMR and Lasso regularization are selected to train the classification model. Thus, in our work, we consider optimal features = features selected by (mRMR ∩ Lasso regularization). Therefore, band-power (13-30 Hz) and wavelet energy of each of the spatially filtered epochs have been selected as the optimal features. We tried to represent the obtained optimal features using scalp plot to find the difference between the MI classes visually. We found that band-power and wavelet energy produce good differentiation between the two classes, as shown in Figure 6. These features are tuned by k-fold cross-validation to create training and testing set.

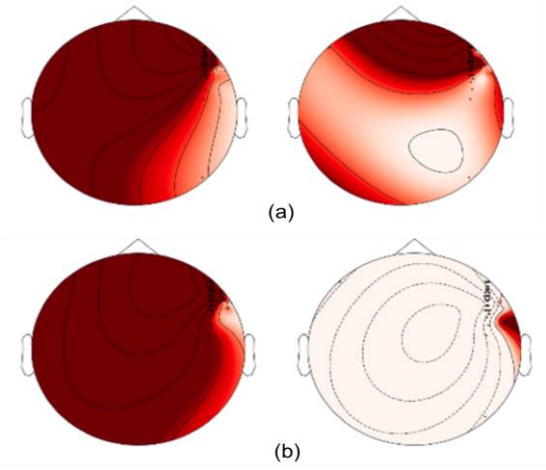

Figure 6. Scalp plot of (a) band-power of right-hand and right-foot MI and (b) wavelet energy for right-hand and right-foot MI.

2.5 Gaussian Naïve Bayes (GNB) Classifier

The Naïve Bayes theorem aims at assigning the class C_i to the feature vector by calculating *a posteriori* probability of the feature vector [38]. Here, $i \in \{H, F\}$, H denotes right-hand and F denotes right-foot MI class. Mathematically, this is defined as:

$$p(C_i|S) = \frac{p(S|C_i) \times p(C_i)}{p(S)} \tag{15}$$

where C_i is the class, $S = \{s_1, s_2, \dots, s_m\}$ is the set of selected optimal features. By assuming Gaussian distribution, Naïve Bayes can be extended as Gaussian Naïve Bayes. Gaussian distribution is easy to work with, because only mean and variance need to be calculated from the training data [39]. Let μ_{jH} and ${\sigma^2}_{jH}$ be the mean and variance value of the feature vector s_j associated with class C_H. Then, the class-conditional probability using Gaussian normal distribution is defined as:

$$p(S = s_j|C_H) = \frac{1}{\sqrt{2\pi{\sigma^2}_{jH}}} e^{-\frac{(s_j-\mu_{jH})^2}{2{\sigma^2}_{jH}}} \tag{16}$$

The prediction result provides the class and is defined as:

$$C_{pred} = \underset{i}{\text{argmax}} \quad p(C_i|s_1, s_2, \dots, s_m) \tag{17}$$

In this study, GNB classifier is used to classify two-class MI signals. The main advantage of this

classifier is that there is no parameter tuning like in other classifiers. The parameters in GNB classifier are automatically calculated by maximum likelihood estimation (MLE) [38].

2.6 Performance Measures

The performance of the proposed method was evaluated using the following measures.

2.6.1 Confusion Matrix

The confusion matrix is a useful tool for analyzing how frequently instances of a class (say X) were correctly classified as class X instances. Having m classes, confusion matrix is a table of size $m \times m$. An entry at (i, j) indicates the number of instances of class i that were labeled by the classifier as class j instances. Here, right-hand instances should be classified as belonging to the right-hand class. Thus, the numbers of true positives (TP), false negatives (FN), false positives (FP) and true negatives (TN) are obtained. For a classifier to have good accuracy, ideally most of the diagonal entries (TP, TN) should have large values with the rest of entries being less or close to zero.

2.6.2 Accuracy

The accuracy is the ratio of total number of correctly classified samples to the total number of samples of all classes.

$$Accuracy = \frac{TP+TN}{TP+FN+FP+TN} \tag{18}$$

2.6.3 κ Score

The κ-score or κ-coefficient is a statistical measure that compares observed accuracy (p_o) with expected accuracy (p_e). The κ-score is given by the following equation:

$$\kappa = \frac{p_o - p_e}{1 - p_e} \tag{19}$$

where, κ = 1 indicates complete agreement between the MI BCI classes, while κ ≤ 0 means that there is no agreement at all.

3. Experiments, Results and Discussion

In this section, the implementation procedure and the experimental results of the proposed method using the dataset IVa of BCI competition III are explained. In this study, the codes were written in Python 2.7, making use of Scikit Learn [40]; a popular machine learning library.

3.1 Performance of the Proposed Method

The given dataset had two MI classes; right-hand and right-foot, to be classified. We experimented with the proposed model using two different numbers of channels. One experiment considered all the 118 channels and the other considered only the 30 channels present over the motor cortex. The optimal features selected from the dataset after applying band-pass filter-based CSP are given as input to the GNB model. Table 4 shows the k-fold cross-validation accuracy of the proposed method for each subject taking 118 and 30 electrodes, respectively. Here, the value of k is taken from 1 to 10; the average and the standard deviation values obtained for all the 10 folds are given in Table 4.

From the values obtained, it is observed that the reduced number of channels gives better accuracy than considering all the 118 channels.

Since we got better accuracy with 30 channels, we proceeded with the experiment with the reduced number of channels. In order to make the evaluation easier, after selecting the optimal features, the training and testing data is created considering all the subject's data together. GNB classifier is built based on the training data and validated using the testing data. Table 5 shows the various performance measures achieved by the proposed method for all the 10 folds.

Table 4. Classification accuracy by *k*-fold cross-validation method for the proposed method.

Subjects	***k*-fold cross-validation accuracy (%) (mean ± std)**	
	118 channels	**30 channels**
aa	93.72±2.81	95.16±1.95
al	89.49±5.73	91.88±4.39
av	91.03±7.22	93.85±4.87
aw	90.48±6.45	94.01±5.62
ay	93.86±3.76	96.65±2.32
Average	**91.72±5.19**	**94.31±3.83**

Table 5. Values of TP, FP, TN and FN of confusion matrix, accuracy (%) and κ score of the proposed method for all the 10 folds.

***k*-folds**	**Confusion Matrix**				**Accuracy (%)**	**κ score**
	TP	**FN**	**FP**	**TN**		
k=1	800	43	39	798	95.12	0.90
k=2	807	39	32	802	95.77	0.92
k=3	805	40	34	801	95.60	0.91
k=4	798	41	40	801	95.18	0.90
k=5	803	40	38	799	95.36	0.91
k=6	799	38	40	803	95.36	0.91
k=7	810	36	32	802	95.95	0.92
k=8	805	41	35	799	95.48	0.91
k=9	808	36	32	804	95.95	0.92
k=10	812	33	28	807	96.37	0.93
Average ± std	**804.7 ± 4.72**	**38.7 ±2.98**	**35 ± 4.11**	**801.6 ±2.67**	**95.61 ± 0.40**	**0.91 ± 0.01**

3.2 Performance Comparison with LDA and SVM Classifiers

The performance of the proposed approach is compared with those of two classifiers; namely, linear discriminant analysis (LDA) [41] and support vector machine (SVM) [42]. LDA and SVM are the most widely used classifiers in MI-based BCI systems. The same optimal features selected to train GNB classifier are used to train these classifiers. The parameters for SVM classifier need to be chosen carefully to avoid under-fitting and over-fitting problems. The outputs obtained by LDA and SVM classifiers are evaluated and compared with the proposed GNB approach. The performance metrics were generated for all the 10 folds. The average and the standard deviation values obtained are shown in Table 6. The result shows that the proposed method provides an improved accuracy over the LDA and SVM classifiers. The runtime of each classifier is noted down, where the values obtained show that the proposed method takes few milliseconds lesser than LDA and SVM methods.

Table 6. Comparison of performance metrics of the proposed method, LDA and SVM classifiers for all the 10 folds (Mean ± Standard deviation**).**

Methods	**Confusion Matrix**				**Accuracy (%)**	**κ score**	**Runtime (in milliseconds)**
	TP	**FN**	**FP**	**TN**			
LDA	752 ± 6.56	71 ± 7.71	71 ± 6.83	786 ± 4.13	91.55 ± 0.75	0.83 ± 0.03	126 ± 4
SVM	778 ± 5.68	54 ± 7.43	56 ± 5.32	792 ± 4.05	93.45 ± 0.63	0.87 ± 0.02	120 ± 5
GNB	**804.7 ± 4.72**	**38.7 ±2.98**	**35 ± 4.11**	**801.6 ±2.67**	**95.61 ± 0.40**	**0.91 ± 0.01**	**118** ± 4

3.3 Discussion

The proposed approach does not require any artifact or noise removal. The band-pass and spatial filtering used in the method itself removes high-and low-frequency artifacts; therefore, there is no need for any explicit artifact removal methods. The results presented in Table 4 prove that the proposed method produces better accuracy with a minimum number of channels. The existing approaches for MI-based EEG data classification make use of high-dimensional feature vectors. The

accuracy achieved may be comparable, but it makes the BCI system slow. The feature selection method used in our work determines the ideal feature set and makes the BCI system work faster. The main advantage of GNB classifier is that there is no parameter tuning. The results listed in Table 6 demonstrate that the GNB classifier with only two feature vectors produces good accuracy and compiles faster than other classifiers. Henceforth, our method proves to be simpler, faster and more accurate for MI-based BCI applications.

4. CONCLUSIONS

In this work, we used a new combination of machine learning approach to classify two-class MI signals for BCI applications. Firstly, the EEG signals with 118 channels are of high dimension. To reduce computational complexity, constraints are applied on selecting channels. Secondly, it is important to note that the EEG signals produce variations among users at different sessions. This inter-subject variability is removed using two different feature selection techniques; namely, mRMR and Lasso regularization. Our results prove that the performance of two-class MI-based BCI can be significantly improved using a few channels and a few feature vectors. This method also reduces computational complexity significantly and increases the speed and accuracy of the classifier models. GNB classifier performed better than the LDA and SVM classifiers. Hence, the proposed approach can be used to design more robust and reliable MI-based real-time BCI applications, like text-entry system, gaming, wheel-chair control, …etc., for motor impaired people. Future work will focus on extending the proposed approach for classifying multi-class MI tasks which can be further used for communication purposes.

REFERENCES

[1] J. Wolpaw and E. W. Wolpaw, Brain-Computer Interfaces: Principles and Practice, Oxford University Press, USA, 2012.

[2] J. R. Wolpaw, N. Birbaumer, D. J. McFarland, G. Pfurtscheller and T. M. Vaughan, "Brain–computer Interfaces for Communication and Control," Clinical Neurophysiology, vol. 113, no. 6, pp. 767–791, 2002.

[3] J. Calderon, Y. Yang, C. Inman, J. Willie and G. Berman, "Decoding Human Behavior from Complex Neural Interactions," Bulletin of the American Physical Society, 2018.

[4] H. M. Golshan, A. O. Hebb, S. J. Hanrahan, J. Nedrud and M. H. Mahoor, "An FFT-based Synchronization Approach to Recognize Human Behaviors Using STN-LFP Signal," IEEE Int'l Conference on Acoustics, Speech and Signal Processing (ICASSP), pp. 979–983, 2017.

[5] H. M. Golshan, A. O. Hebb, S. J. Hanrahan, J. Nedrud and M. H. Mahoor, "A Hierarchical Structure for Human Behavior Classification Using STN Local Field Potentials," Journal of Neuroscience Methods, vol.293, pp.254–263, 2018.

[6] S. R. Sreeja, V. Joshi, S. Samima, A. Saha, J. Rabha, B. S. Cheema, D. Samanta and P. Mitra, "BCI Augmented Text Entry Mechanism for People with Special Needs," The 8th Int'l Conference on Intelligent Human Computer Interaction (IHCI), pp. 81-93, 2016.

[7] B. Blankertz, S. Lemm, M. Treder, S. Haufe and K. R. Muller, "Single-trial Analysis and Classification of ERP Components- A Tutorial," NeuroImage, vol. 56, no. 2, pp. 814–825, 2011.

[8] B. He, B. Baxter, B. J. Edelman, C. C. Cline and W. Y. Wenjing, "Non-invasive Brain-Computer Interfaces Based on Sensorimotor Rhythms," Proc. of the IEEE, vol. 103, no. 6, pp. 907–925, 2015.

[9] G. Pfurtscheller and C. Neuper, "Motor Imagery and Direct Brain-Computer Communication," Proceedings of the IEEE, vol. 89, no. 7, pp. 1123–1134, 2001.

[10] H. Ramoser, J. Muller-Gerking and G. Pfurtscheller, "Optimal Spatial Filtering of SingleTtrial EEG during Imagined Hand Movement," IEEE Trans. Rehabilitation Engg., vol. 8, no. 4, pp. 441–446, 2000.

[11] S. Lemm, B. Blankertz, G. Curio and K. R. Muller, "Spatio-spectral Filters for Improving the Classification of Single Trial EEG," IEEE Trans. Biomedical Engg., vol. 52, no. 9, pp. 1541–1548, 2005.

[12] R. Tomioka, G. Dornhege, G. Nolte, B. Blankertz, K. Aihara and K. R. Muller, "Spectrally weighted common spatial pattern algorithm for single trial EEG classification," Department of Mathematical

Informatics, University of Tokyo, Japan, Tech. Rep., vol. 40, 2006.

[13] W. Wu, X. Gao, B. Hong and S. Gao, "Classifying Single-trial EEG during Motor Imagery by Iterative Spatio-spectral Patterns Learning (ISSPL)," IEEE Trans. Biomedical Engg., vol. 55, no. 6, pp.1733–1743, 2008.

[14] H. Higashi and T. Tanaka, "Simultaneous Design of FIR Filter Banks and Spatial Patterns for EEG Signal Classification," IEEE Trans. on Biomedical Engg., vol. 60, no. 4, pp. 1100–1110, 2013.

[15] C. Park, C. C. Took and D. P. Mandic, "Augmented Complex Common Spatial Patterns for Classification of Noncircular EEG from Motor Imagery Tasks," IEEE Trans. Neural Systems and Rehabilitation Engg., vol. 22, no. 1, pp. 1–10, 2014.

[16] A. S. Aghaei, M. S. Mahanta and K. N. Plataniotis, "Separable Common Spatio-spectral Patterns for Motor Imagery BCI Systems," IEEE Trans. on Biomedical Engg., vol. 63, no. 1, pp. 15–29, 2016.

[17] D. Li, H. Zhang, M. S. Khan and F. Mi, "A Self-Adaptive Frequency Selection Common Spatial Pattern and Least Squares Twin Support Vector Machine for Motor Imagery Electroencephalography Recognition," Biomedical Signal Processing and Control, vol. 41, pp. 222–232, 2018.

[18] Y. Li, P. P. Wen et al., "Modified CC-LR Algorithm with Three Diverse Feature Sets for Motor Imagery Tasks Classification in EEG-Based Brain–Computer Interface," Computer Methods and Programs in Biomedicine, vol. 113, no. 3, pp. 767–780, 2014.

[19] C. Vidaurre, N. Kramer, B. Blankertz and A. Schlogl, "Time Domain Parameters as a Feature for EEG-Based Brain–Computer Interfaces," Neural Networks, vol. 22, no. 9, pp. 1313–1319, 2009.

[20] P. Herman, G. Prasad, T. M. McGinnity and D. Coyle, "Comparative Analysis of Spectral Approaches to Feature Extraction for EEG-based Motor Imagery Classification," IEEE Trans. Neural Systems and Rehabilitation Engg., vol. 16, no. 4, pp. 317–326, 2008.

[21] W.-Y. Hsu and Y.-N. Sun, "EEG-based Motor Imagery Analysis Using Weighted Wavelet Transform Features," Journal of Neuroscience Methods, vol. 176, no. 2, pp. 310–318, 2009.

[22] M. Tavakolan, X. Yong, X. Zhang and C. Menon, "Classification Scheme for Arm Motor Imagery," Journal of Medical and Biological Engg., vol. 36, no. 1, pp. 12–21, 2016.

[23] Y. Zhang, G. Zhou, J. Jin, X. Wang and A. Cichocki, "Optimizing Spatial Patterns with Sparse Filter Bands for Motor Imagery-based Brain–Computer Interface," Journal of Neuroscience Methods, vol. 255, pp. 85–91, 2015.

[24] H. Wang, Y. Zhang, N. R. Waytowich, D. J. Krusienski, G. Zhou, J. Jin, X. Wang and A. Cichocki, "Discriminative feature extraction *via* multivariate linear regression for SSVEP-based BCI," IEEE Trans. Neural Systems and Rehabilitation Engg., vol. 24, no. 5, pp. 532–541, 2016.

[25] F. Lotte, M. Congedo, A. L´ecuyer, F. Lamarche and B. Arnaldi, "A Review of Classification Algorithms for EEG-based Brain–Computer Interfaces," Jo. of Neural Engg., vol. 4, no. 2, p. R1, 2007.

[26] Y. Zhang, G. Zhou, J. Jin, Q. Zhao, X. Wang and A. Cichocki, "Sparse Bayesian Classification of EEG for Brain–Computer Interface," IEEE Transactions on Neural Networks and Learning Systems, vol. 27, no. 11, pp. 2256–2267, 2016.

[27] V. P. Oikonomou, A. Maronidis, G. Liaros, S. Nikolopoulos and I. Kompatsiaris, "Sparse Bayesian Learning for Subject Independent Classification with Application to SSVEP-BCI," The 8th Int'l IEEE/EMBS Conf. Neural Engineering (NER), pp. 600–604, 2017.

[28] Y. Zhang, G. Zhou, J. Jin, Y. Zhang, X. Wang and A. Cichocki, "Sparse Bayesian Multiway Canonical Correlation Analysis for EEG Pattern Recognition," Neurocomputing, vol. 225, pp. 103–110, 2017.

[29] Y. Zhang, Y. Wang, J. Jin and X. Wang, "Sparse Bayesian Learning for Obtaining Sparsity of EEG Frequency Bands-based Feature Vectors in Motor Imagery Classification," Int'l Journal of Neural Systems, vol. 27, no. 02, p. 1650032, 2017.

[30] "BCI Competition III", [Online], Available: http://www.bbci.de/competition/iii

[31] L. He, D. Hu, M. Wan, Y. Wen, K. M. von Deneen and M. Zhou, "Common Bayesian Network for Classification of EEG-based Multiclass Motor Imagery BCI," IEEE Trans. Systems, Man and Cybernetics: Systems, vol. 46, no. 6, pp. 843–854, 2016.

[32] W.-K. Tam, K.-Y. Tong, F. Meng and S. Gao, "A Minimal Set of Electrodes for Motor Imagery BCI to Control an Assistive Device in Chronic Stroke Subjects: A Multi-Session Study," IEEE Trans. Neural

Systems and Rehabilitation Engg., vol. 19, no. 6, pp. 617–627, 2011.

[33] M. H. Alomari, E. A. Awada, A. Samaha and K. Alkamha, "Wavelet-based Feature Extraction for the Analysis of EEG Signals Associated with Imagined Fists and Feet Movements," Computer and Information Science, vol. 7, no. 2, p. 17, 2014.

[34] X. Zhang, L. Yao, D. Zhang, X. Wang, Q. Z. Sheng and T. Gu, "Multi-person Brain Activity Recognition *via* Comprehensive EEG Signal Analysis," arXiv preprint arXiv:1709.09077, 2017.

[35] H. Peng, F. Long and C. Ding, "Feature Selection Based on Mutual Information Criteria of Max-dependency, Max-relevance and Min-redundancy," IEEE Trans. Pattern Analysis and Machine Intelligence, vol. 27, no. 8, pp. 1226–1238, 2005.

[36] J. Gui, Z. Sun, S. Ji, D. Tao and T. Tan, "Feature Selection Based on Structured Sparsity: A Comprehensive Study," IEEE Trans. Neural Networks and Learning Systems, vol. 28, no. 7, pp. 1490–1507, 2017.

[37] P. Zhao and B. Yu, "On Model Selection Consistency of Lasso," Journal of Machine Learning Research, vol. 7, no. Nov., pp. 2541–2563, 2006.

[38] I. H. Witten, E. Frank, M. A. Hall and C. J. Pal, Data Mining: Practical Machine Learning Tools and Techniques, Morgan Kaufmann, 2016.

[39] K. S. Kassam, A. R. Markey, V. L. Cherkassky, G. Loewenstein and M. A. Just, "Identifying Emotions on the Basis of Neural Activation," PloS one, vol. 8, no. 6, p. e66032, 2013.

[40] Scikit-learn, "Machine Learning in Python", [Online], Available: http://scikit-learn.org/

[41] B. Blankertz, R. Tomioka, S. Lemm, M. Kawanabe and K.-R. Muller, "Optimizing Spatial Filters for Robust EEG Single-trial Analysis," IEEE Signal Processing Magazine, vol. 25, no. 1, pp. 41–56, 2008.

[42] S. Siuly and Y. Li, "Improving the Separability of Motor Imagery EEG Signals Using a Cross Correlation-based Least Square Support Vector Machine for Brain–Computer Interface," IEEE Trans. Neural Systems and Rehabilitation Engg., vol. 20, no. 4, pp. 526–538, 2012.

ملخص البحث:

في أكثر الأحوال، تكون لدى الأشخاص المعاقين حركياً صعوبات في التواصل مع المجتمع. ويمكن للبينيّات التي تربط الدماغ والحاسوب أن تعيد شيئاً من الأمل لهؤلاء. وتشكل إشارات التصوير الحركي المسجلة بواسطة المخططات الدماغية الكهربائية الأساس الأكثر ملاءمة لتصميم بينيّات الدماغ-الحاسوب، لأنها توفر درجة أعلى من الحرية. وتساعد بينيّات الدماغ-الحاسوب القائمة على التصوير الحركي الأشخاص على التفاعل مع أي من تطبيقاتها عبر أداء سلسلة من مهمات التصوير الحركي. إلا أن هناك عدداً من التحديات، منها: اختلاف ملاءمتها من شخص لآخر، واستخلاص خصائصها المعيّنة للمستخدم، وزيادة دقتها.

وتقترح هذه الدراسة طريقة للتغلب على المشكلات المذكورة، حيث نقترح طريقة تأخذ بعين الاعتبار: اختيار القنوات، والنمط المكاني المشترك القائم على استخدام مرشِّح تمرير نطاق ترددي، واستخلاص واختيار الخصائص، والنمذجة باستخدام مصنِّف بايز الغاوسي البسيط. ونظراً لأنه يتم اختيار الخصائص الأمثل عن طريق تقنيات اختيار الخصائص، فإن ذلك يساعد في التغلب على مسألة اختلاف ملاءمة البينيّات من شخص لآخر ويؤدي الى تحسين أداء المصنِّف. وتم التحقق من نجاعة الطريقة المقترحة باستخدام مجموعة البيانات (IVa)، كما جرت مقارنة المصنِّف المستخدم في هذه الدراسة بمصنِّفين آخرين هما: (LDA و SVM). وأثبتت النتائج تفوق المصِّف المقترح من حيث الدقة.

كذلك يمكن تطوير الطريقة المقترحة مستقبلاً لتصميم تطبيقات موثوقة وفي الزمن الحقيقي لبينيّات الدماغ-الحاسوب المستندة الى التصوير الحركي.

Jordanian Journal of Computers and Information Technology (JJCIT), Vol. 04, No. 02, August 2018.

PATH LOSS ESTIMATION FOR BONE IMPLANTABLE APPLICATIONS

Rula Alrawashdeh

(Received: 5-Jan.-2018, Revised: 24-Mar.-2018, Accepted: 9-Apr.-2018)

ABSTRACT

The implantable body sensor network (IBSN) has many promising applications. The sensors in the network support different functionalities, such as glucose monitoring and strain measurement in bones. These sensors work with a central hub that communicates with a receiver outside the body. A reliable communication link between these sensors is essential. In this paper, the path loss between elliptic circular loop antennas in muscle and two different bones (the humerus and femoral bone) has been estimated at 403 MHz inside the CST Katja voxel body model. A 33 dB larger path loss is obtained between muscle and humerus antennas than that between muscle and femoral bone antennas. Hence, a standard link with an ideal phase shift keying (PSK) can be only built up from the femoral bone to the the muscle above the hip. The results in this paper provide a good source of data for link budget calculations for bone implantable applications.

KEYWORDS

EIRP, IBSN, ISM, MedRadio, PSK.

1. INTRODUCTION

Implantable devices have many important applications in healthcare and biomedical telemetry [1]-[2]. An antenna is normally used with the implantable device to transfer the biological data wirelessly from this device to a receiver [3]-[4]. The receiver is placed at different positions (in the human body, on or outside of it) to suit different applications. Hence, different communication links (in-in, in-on and in-off body) can be established [5]-[11]. These links should be characterized and their losses should be carefully estimated. The path loss between implantable and off-body antennas was estimated in [9]. It was also estimated between implantable and on-body antennas in [6]-[7]. In implantable body sensor network (IBSN), different implantable sensors can exist and work with each other. For example, a glucose monitoring implant can work with a pacemaker/central hub, which then can communicate with a receiver placed outside the human body. This is very beneficial, as the communication from inside the human body to an external receiver needs to take place from one implant only [5], [12]. However, the path loss should be evaluated in anatomical body models considering actual and exact positions of implantations, in order to obtain accurate results. The path loss between different muscle implants was estimated in [12]-[13] using flexible dipole antennas at 2.45 GHz. In [14], the path loss was experimentally measured within 2.36-2.5 GHz in a homogeneous liquid body phantom of small dimensions ($30\times 30\times 20$ cm^3). However, the losses in that paper were measured for paths in a simplified body phantom that did not provide a good resemblance of the real human body. In [11], a communication link between a transmitting half-wave dipole in the pancreas tissue and a probe receiver placed in different points in the human mesh was characterized at 2.45 GHz and its path loss was modeled. The 401-406 MHz Medical Device Radiocommmunication Service (MedRadio) band is mainly allocated for implantable applications. The attenuation in the human body tissues within the MedRadio band is smaller than that within the 2.45 GHz Industrial Scientific and Medical (ISM) band. The path loss in this band was estimated in [5] and [11] at 402.5 and 403 MHz, respectively. However, none of these paths was in bones or between bone and muscle implantable antennas. Bone implants have many important applications, such as bone healing, growth and checkups of artificial joints [15]-[16]. Different antenna designs were proposed for bone implants [17]-[21]. Bone implants may exist with other muscle implants in the IBSN. Therefore, it is very beneficial to quantify the losses of communication paths between bone and muscle implants for different applications.

Rula Alrawashdeh is with Department of Electrical Engineering, Mutah University, Alkarak, Jordan. Email: rularsr18@gmail.com

In this paper, the path loss between bone and muscle implantable loop antennas has been estimated and quantified at 403 MHz inside simplified and anatomical Katja voxel body models. The implantable antennas are first designed in simplified body models to accelerate the overall design process. Then, they are simulated in the anatomical body model to obtain accurate results about the path losses. The bone implantable antenna is placed inside the humerus or femoral bone, while the muscle implantable antenna is placed in the muscle above the left hip.

This paper is organized as follows: First, the design of both antennas in the simplified body model is presented. Then, performance of antennas is evaluated and validated in the CST Katja voxel body model. After that, the losses of the communication paths between muscle and bone antennas are estimated and the link budgets are calculated. Finally, the paper is concluded.

2. SETUP AND CONFIGURATION

Flexible elliptic circular loop antennas are used for the analysis in this paper. This is because loop antennas are more efficient in the lossy human body than electrical type antennas [22]-[24]. The antenna is bent around cylindrical implants of the following dimensions:

5 mm in radius and 11 mm in length for the glucose monitoring implant in the muscle above the left hip.
8 mm in radius and 56 mm in length for the implant in the humerus and femoral bone.

Both antennas have the same shape as shown in Figure 1. However, they have different dimensions as summarized in Table 1.

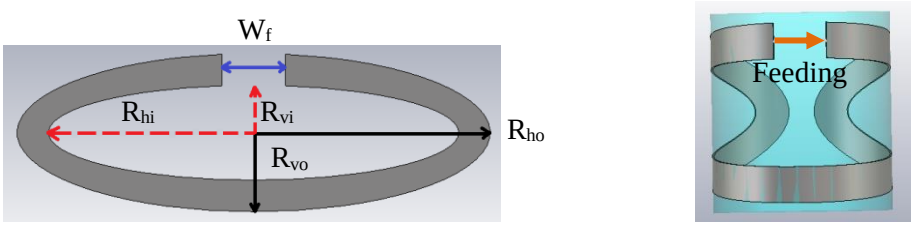

(a) (b)

Figure 1. The proposed antennas structure: (a) flat, (b) bent views.

Table 1. The dimensions of the proposed antennas.

Parameter	**Symbol**	**Dimensions (mm)**	
		Muscle implantable antenna	**Bone implantable antenna**
The outer horizontal radius	R_{ho}	15	28
The inner horizontal radius	R_{hi}	13	23
The outer vertical radius	R_{vo}	5	18
The inner vertical radius	R_{vi}	3	17
Feeding gap width	W_f	3	4

Bone implants are usually larger in size than muscle implants [16], [21] and hence the bone implantable antenna is designed with larger physical dimensions.

The human body tissues are lossy and their dielectric properties are frequency dependent. The antennas are simulated in the middle of simplified human body models. These models are conical in shape and have the following properties:

- Of a single homogeneous layer of ($\varepsilon_r = 57.1$ and $\sigma = 0.79\ S/m$ which resembles the dielectric properties of muscle at 403 MHz [25]). The antenna intended for implantation in the muscle above the left hip is designed inside of this body model.
- Of two layers; outer muscle layer of ($\varepsilon_r = 57.1$ and $\sigma = 0.79\ S/m$) and inner bone layer of ($\varepsilon_r = 13.14$ and $\sigma = 0.09\ S/m$), which resemble the dielectric properties of muscle and bone cortical, respectively at 403 MHz [25]. The antenna intended for implantation in the humerus and femoral bone is designed in the middle of the bone layer of this model.

Top and side views of the simplified human body models are shown in Figure 2.

The simplified body models are much smaller in size than the anatomical body models. They are also of uniform layers, as indicated above. Therefore, the simulation time inside of these models is much shorter than that in the anatomical body models. Hence, the overall design process will be accelerated if the antenna structure is optimized first in the simplified body model and then evaluated in the anatomical body model [5, 22, 26]. The antenna performance may be altered in the anatomical body model, which has a better resemblance of the real human body. However, if the antenna is broad in bandwidth, its matching will be maintained (S11≤ -10 dB) within the band of interest (401-406 MHz MedRadio band for the case of this paper) [5]. Also, the process of optimizing the antenna structure in the simplified body helps in understanding the antenna structure and its effective parameters. Hence, small modifications are only expected to be made in the anatomical body model if needed.

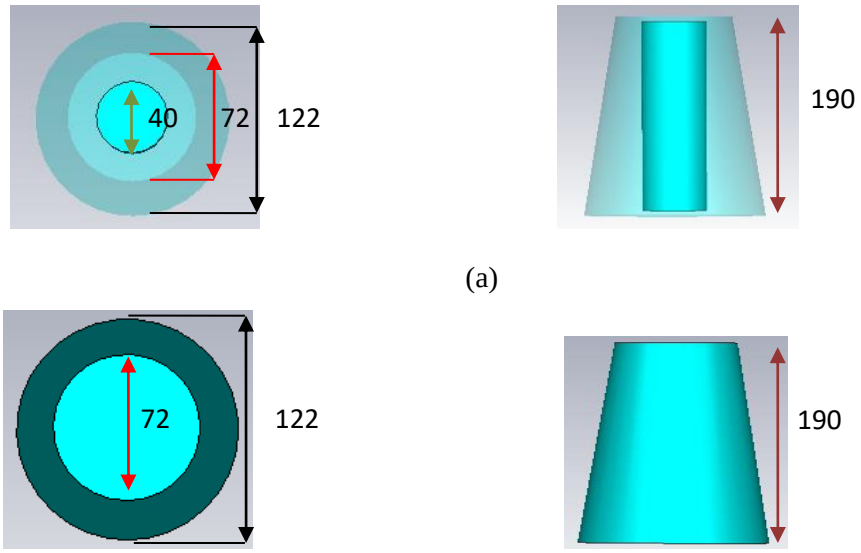

Figure 2. Top and side views of the: (a) two-layer (bone-muscle) and (b) single-muscle layer simplified body model; dimensions in mm.

3. PERFORMANCE

In this section, the simulated reflection coefficient S11 and realized gain of the proposed antennas will be evaluated and discussed in the simplified and CST Katja voxel body models.

3.1 Performance in the Simplified Body Model

The proposed antennas are simulated at the centre of the simplified body models. Simulations are conducted using the CST microwave studio [27]. Hexahedral meshes are employed and a minimum distance of λ/8 is kept between the structure and the edge of the simulation space. The antennas are fed by discrete ports of 50 Ω with an input power of 1 W. The antenna is designed to obtain a broad bandwidth of wider than 200 MHz around 403 MHz. This is to guarantee a robust performance of the antenna if detuning happens in the anatomical and actual human bodies. The simulation results are shown in Figure 3. Both antennas obtain good matching (S11≤ -10 dB) at 403 MHz. The realized gain values for the simulated antennas are -22 and -35.61 dBi for the bone and muscle implantable antennas, respectively at 403 MHz. The bone implantable antenna has obtained a larger gain than that for the muscle implantable antenna. This is because the bone implant is larger in size than the muscle implant. Hence, the lossy area surrounding it will be smaller than that surrounding the muscle implant. Moreover, the bone has a smaller conductivity than that for muscle ($\sigma = 0.09$ and 0.79 S/m for bone cortical and muscle, respectively [25]). This reduces the near field coupling between the antenna and the surrounding human body tissue which reduces the power loss due to absorption. Hence, a larger gain is obtained. The muscle implantable antenna has obtained a good matching (S11≤-10 dB) as desired. Although the antenna bandwidth is not centered at 403 MHz, a good matching is expected to be maintained in the anatomical body model. This

is because the antenna is intended for implantation in the area above the left hip in close proximity to some organs of the digestive tract, such as the small intestine. The relative permittivity of these organs is larger than that for muscle (57.1 for muscle and 66 for the small intestine at 403 MHz [25]) and hence the resonant frequency is expected to be the same or shifted down, but not shifted up in the anatomical body model. It will be shown in a following section that S11 is also smaller than -10 dB at 403 MHz in the anatomical body model, as expected.

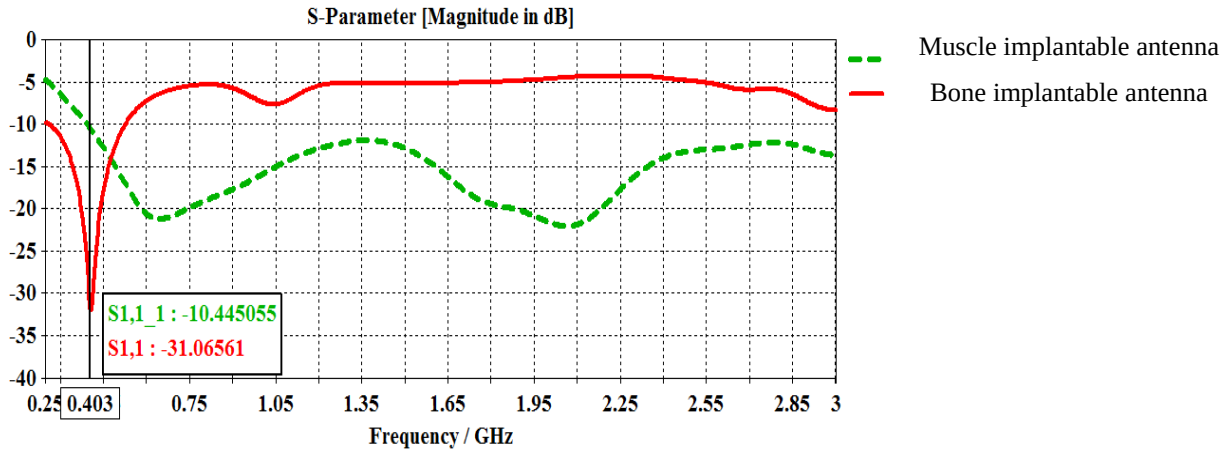

Figure 3. The reflection coefficient S11 (dB) for the muscle and bone implantable antennas in the simplified body models.

3.2 Performance in the Anatomical Body Model

In order to estimate the path loss accurately, it is very important to simulate the antennas at the exact positions of implantations inside the anatomical body model. The anatomical body model is composed of non-uniform and heterogeneous tissues that resemble the real human body tissues [28]. These models are provided by different simulation tools, such as CST. The CST Katja voxel body model is used for the simulations in this paper. The CST Katja voxel body model represents a 43-year old female with height of 163 cm and weight of 62 kg [29]. The bone implantable antenna in this paper is placed in the humerus or femoral bone, while the muscle implantable antenna is placed in the muscle above the left hip. It is worth indicating that in order to provide accurate comparison, the same antenna is simulated in the humerus and femoral bone. The positions of implantation in the anatomical body model are shown in Figures 4 and 5. The muscle implantable antenna is placed in the muscle above the left hip, directly beneath the fat layer. Bone implantable antennas are placed at the centre of the humerus and femoral bones. All antennas are oriented to the front such as in Figure 1 (b).

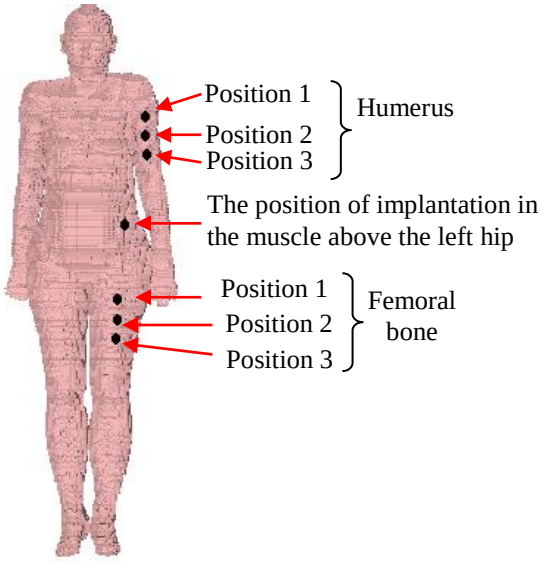

Figure 4. Positions of implantation in the CST Katja voxel body model (front view of the human body).

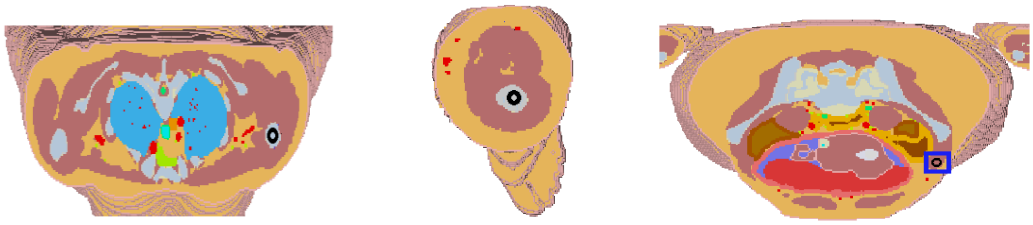

Figure 5. Positions of implantation (indicated by the black ring) in the CST Katja voxel body model (top view).

Two links are first simulated at 403 MHz. One between the implantable antenna in the humerus at position 1, which is 15 mm above the armpit, and the antenna in the muscle above the left hip. The other one is established between the antenna in the femoral bone at position 1, which is at 20 mm from the top of the femoral bone, and the antenna in the muscle above the left hip. The antenna in the muscle above the left hip is simulated at a fixed position which is shown in the figure. This position is popular for glucose monitoring implants [5], [21]. The results of the simulated reflection coefficient are shown in Figure 6.

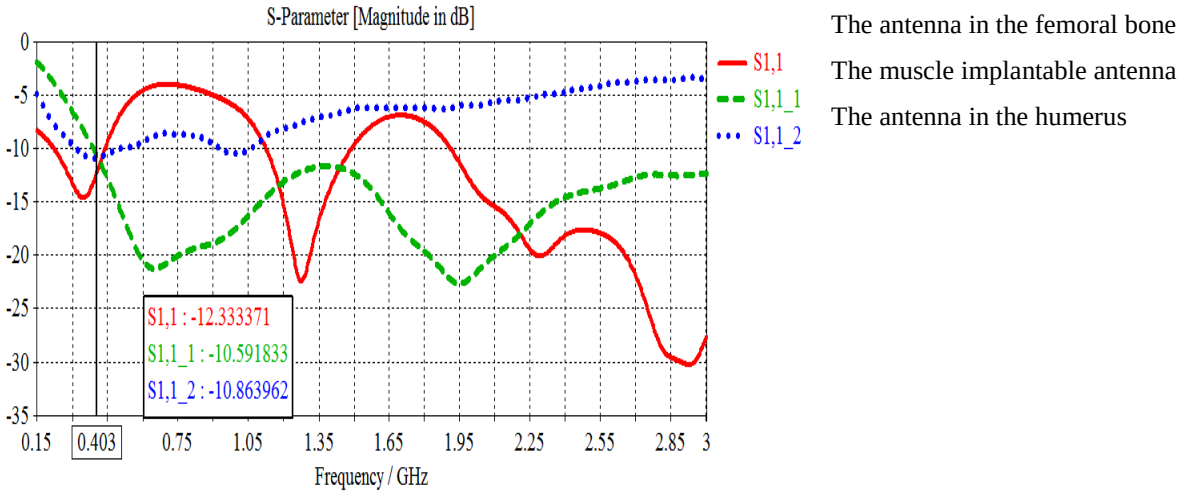

Figure 6. The reflection coefficient S11 (dB) for the muscle and bone implantable antennas at position 1 in the CST Katja voxel body model.

The results in the figure show that a good matching (S11≤ -10 dB) is obtained at 403 MHz for all of the three cases of implantation in the muscle and both bones. To provide more options for actual implantation in the human body, two other positions of implantation in the humerus and femoral bones are attempted (positions 2 and 3 shown in Figure 4). A distance of 10 mm is kept between the two positions. The simulated reflection coefficient obtained a good matching (S11≤ -10 dB) for all of these positions.

4. Path Loss Estimation and Link Budget Calculations

This section aims at estimating the losses of both of the communication links indicated above and calculating the corresponding link budget.

4.1 Simulated Path Losses and Link Parameters

The path loss (P_L) is defined as the inverse of the transmission coefficient (S_{21}) between the transmitting and receiving implantable antennas, which are matched to 50 Ohms (1) [12].

$$P_L\left(dB\right)=\left(\frac{P_{in}}{P_{Rx}}\right)=-10\log_{10}\left|S_{21}\right|^2=-\left|S_{21}\right|\left(dB\right) \quad (1)$$

where P_{in} (W) is the power input to the transmitting antenna and P_{Rx} (W) is the power received at the receiving antenna.

The simulated path losses between the transmitting and receiving antennas investigated in this paper are summarized in the Table 2.

Table 2. The muscle-humerus and muscle-femoral bone path loss P_L (dB) at the three positions of implantation.

	Position 1	**Position 2**	**Position 3**
Muscle - humerus	123 dB	121.4	120
Muscle - femoral bone	86.15	87.8	90

The largest path loss is obtained at position 1 and position 3 at the humerus and femoral bone, respectively. The distance between the muscle and bone implantable antennas at these positions is the largest amongst all cases of the three positions of investigation. When the distance increases, the path loss increases accordingly.

A link of the parameters summarized in Table 3 is considered. This link was considered in [12] to evaluate the communication path links between muscle implantable devices. The links investigated in this paper will be also evaluated based on the parameters of this link.

Table 3. Parameters of a communication link between muscle and bone implantable devices.

Link parameter	**Value**
Transmitted power, P_{TX} (μW)	25
Ambient temperature, AT (K)	310
Bit rate, B_r (Kb/s)	7
Boltzmann's constant, K_B (J/K)	1.38×10^{-23}
Coding gain, G_c (dB)	0
Fixing or deterioration gain, G_d (dB)	2.5
Energy per bit to noise power spectral density ratio, E_b/N_0 (dB) (ideal PSK)	9.6
Noise spectral density, N_0 (dBm/Hz)	-173
Bit error rate (BER)	1×10^{-5}

The power is limited to up to 25 μW in the 401-406 MHz MedRadio band [30] to prevent hazardous heating of the biological tissues. Phase Shift Keying (PSK) modulation is assumed. In terms of bit error rate (BER), PSK exhibits considerable advantage over Frequency Shift Keying (FSK) and Amplitude Shift Keying (ASK) at the same amplitude levels [31]. The coding is assumed to present no gain to the system for worst-case consideration.

4.2 Link Budget Calculations

The communication is build up when the link carrier to noise density $(\frac{C}{N_0})$ exceeds the required $(\frac{C}{N_0})$ referring to Eqs. (2 and 3) [12]:

$$\text{Link}\left(\frac{C}{N_0}\right)(dB) = P_{TX}\,(dB) - P_{L,organ}\,(dB) - N_0(dB) \quad (2)$$

$$\text{Required}\left(\frac{C}{N_0}\right)(dB) = \left(\frac{E_b}{N_0}\right)(dB) + 10\,log_{10}(B_r) - G_c(dB) + G_d(dB) \quad (3)$$

Considering the link parameters in Table 3, the required $\left(\frac{C}{N_0}\right)$ is calculated as 50.55 dB. The link $\left(\frac{C}{N_0}\right)$ should be larger than 50.55 dB for this communication to build up. To satisfy this, the path loss should be samller than 106.45 dB. This can be obtained for the communication link between the glucose monitoring implant in the muscle above the left hip and the implant in the femoral bone for all of the investigated locations, but not with that for any location in the humerus.

5. CONCLUSIONS

In this paper, the path loss between a glucose monitoring implant and bone implants in the humerus and

femoral bone has been estimated and quantified. The glucose monitoring implant is simulated in the muscle above the left hip. The path loss increases with distance. Therefore, the path loss of the link from the humerus to the glucose monitoring implant is larger than that from the femoral bone. A loss of up to 123 dB is obtained for the path between the implant in the muscle above the left hip and that in the humerus. A loss of up to 90 dB is obtained between the implant in the muscle above the left hip and that in the femoral bone. Based on the results in this paper, it can be concluded that a glucose monitoring implant in the muscle above the left hip can communicate with the implant in the femoral bone, but not with that in the humerus considering the parameters of a typical communication link between implants based on PSK modulation. For future work, different channels between the femoral bone and other implants for different applications will be fully characterized and their path losses will be modelled.

REFERENCES

[1] K. D. Barnard, "Acceptability of Implantable Continuous Glucose Monitoring Sensor," Jou. Diabetes Sci. Technol., vol. 2017, Oct. 2017.

[2] H. Belham et al., "Implantable Strain Sensor to Monitor Fracture Healing with Standard Radiography," Scientific Report, vol. 7, no. 1489, May 2017.

[3] K. Zhang, C. Liu, X. Liu, H. Guo and X. Yang, "Miniaturized Circularly Polarized Implantable Antenna for ISM-Band Biomedical Devices," International Journal of Antennas and Propagation, vol. 2017, pp. 1-9, March 2017.

[4] M. Kod et al., "Feasibility Study of Using the Housing Cases of Implantable Devices as Antennas," IEEE Access, vol. 4, pp. 6939-6949, Sep. 2016.

[5] R. Alrawashdeh, Implantable Antennas for Biomedical Applications, Ph.D. Dissertation, Dept. Elect. Eng., Liverpool Univ., Liverpool, UK, 2015.

[6] P. A. Floor et al., "In-Body to On-Body Ultra-wideband Propagation Model Derived from Measurements in Living Animals," IEEE Jou. of Biomedical and Health Informatics, vol. 19, no. 3, pp. 938-948, May 2015.

[7] A. Stango, K. Y. Yazdandoost, F. Negro and D. Farina, "Characterization of In-Body to On-Body Wireless Radio Frequency Link for Upper Limb Prostheses," PLoS One 11(10): e0164987, Oct. 2016.

[8] A. Alomainy and Y. Hao, "Modeling and Characterization of Biotelemetric Radio Channel from Ingested Implants Considering Organ Contents," IEEE Transactions on Antennas and Propagation, vol. 57, no. 4, pp. 999-1005, April 2009.

[9] D. Kurup, G. Vermeeren, E. Tanghe, W. Joseph and L. Martens, "In-to-Out Body Antenna-Independent Path Loss Model for Multi-layered Tissues and Heterogeneous Medium," Sensors, vol. 15, pp. 408-421, Jan. 2015.

[10] Y. Liao, M. S. Leeson and M. D. Higgins, "A Communication Link Analysis Based on Biological Implant Wireless Body Area Networks," Applied Computational Electromagnetics Society Journal, June 2016.

[11] T. Chrysikos, I. Zisi and S. Kotsopoulos, "Channel Modeling and Path Loss Characterization for In-body Propagation at MICS and ISM Bands," Wireless Telecommunication Symposium (WTS 2016), London, pp. 1-7, 2016.

[12] D. Kurup, W. Joseph, G. Vermeeren and L. Martens, "Specific Absorption Rate and Path Loss in Specific Body Location in Heterogeneous Human Model," IET Microwaves, Antennas & Propagation, vol. 7, no. 1, pp. 35-43, Jan. 2013.

[13] D. Kurup et al., "In-Body Path Loss Models for Implants in Heterogeneous Human Tissues Using Implantable Slot Dipole Conformal Flexible Antennas", EURASIP Journal on Wireless Communications and Networking, vol. 2011, no. 54, pp. 1-9, 2011.

[14] R. Chavez-Santiago et al., Experimental Path Loss Models for In-Body Communications within 2.36–2.5 GHz, IEEE Journal of Biomedical and Health Informatics, vol. 19, no. 3, pp. 930-937, May 2015.

[15] Guide to Knee Replacement Implants and Their Manufacturers, [Online], Available: https://www.healthline.com/health/total-knee-replacement-surgery/implant-manufacturers

[16] J. A. López-López et al., "Choice of Implant Combinations in Total Hip Replacement: Systematic Review and Network Meta-analysis," BMJ, Nov. 2017.

[17] D. Karnaushenko, D. Makarov and O. G. Schmidt, "Compact Helical Antenna for Smart Implant Applications," NPG Asia Mterials 7, June 2015.

[18] R. Alrawashdeh, Y. Huang and P. Cao, "A Flexible Loop Antenna for Total Knee Replacement Implants in the MedRadio Band," Proc. LAPC, Loughborough, UK, pp. 225-228, 2013.

[19] P. Zakavi, N. C. Karmakar and I. Griggs, "Wireless Orthopedic Pin for Bone Healing and Growth: Antenna Development," IEEE Transactions on Antennas and Propagation, vol. 58, no. 12, pp. 4069-4074, Dec. 2010.

[20] S. Symeonidis, W. G. Whittow, C. Panagamuwa and M. Zecca, "An Implanted Antenna System for the Monitoring of the Healing of Bone Fractures," Loughborough Antennas & Propagation Conference (LAPC 2015), Loughborough, pp. 1-4, 2015.

[21] M. K. Magill, G. A. Conway and W. G. Scanlon, "Robust Implantable Antenna for In-body Communications," Loughborough Antennas & Propagation Conference (LAPC 2015), Loughborough, pp. 1-4, 2015.

[22] F. Merli, Implantable Antennas for Biomedical Applications, Ph.D. Dissertation, Dept. Elect. Eng., EPFL Univ., Lausanne, Switzerland, 2011.

[23] R. Alrawashdeh, "A Review on Wireless Power Transfer in Free Space and Conducting Lossy Media," Jordanian Journal of Computers and Information Technology (JJCIT), vol. 3, no. 2, pp. 71-88, Aug. 2017.

[24] Y. El-Saboni, G. A. Conway and W. G. Scanlon, "The Importance of Antenna Near-Field Losses in Intra-Body UHF Communication Applications," IEEE International Symposium on Antennas and Propagation & USNC/URSI National Radio Science Meeting, San Diego, CA, pp. 399-400, 2017.

[25] "Calculation of the Dielectric Properties of Body Tissues," Institute for Applied Physics, Italian National Research Council, [Online], Available: http://niremf.ifac.cnr.it/tissprop/

[26] A. Kiourti and K. S. Nikita, "Methodologies for Fast and Accurate Design of Implantable Antennas: Analysis and Comparison," 7th European Conference on Antennas and Propagation (EuCAP 2013), Gothenburg, pp. 579-582, 2013.

[27] CST - Computer Simulation Technology, [Online], Available: http://www.CST.com

[28] R. Alrawashdeh, Y. Huang and Q. Xu, "Evaluation of Implantable Antennas in Anatomical Body Models," CST-article 2014.

[29] CST Studio Suite, BioEM Simulation Using CST STUDIO SUITE 2013, [Online], Available: https://www.cst.com/Content/Events/downloads/euc2013/5-4-2_CST_EUC.pdf

[30] Electromagnetic Compatibility and Radio Spectrum Matters (ERM); Short-Range Devices (SRD); Ultra-Low Power Active Medical Implants (ULP-AMI) and Peripherals (ULP-AMI-P) Operating in the Frequency Range 402 MHz to 405 MHz; Part 1 and Part 2, European Telecommunications Standards Institute (ETSI) Std. EN 301 839-1/2 V1.3.1, 2007, [Online], Available: www.etsi.org

[31] F. Asgarian and A. M. Sodagar, "Wireless Telemetry for Implantable Biomedical Microsystems," Biomedical Engineering Trends in Electronics, Communications and Software, InTech, pp. 21-45, Jan. 2011.

ملخص البحث:

هناك الكثير من التطبيقات الواعدة لشبكة المجسات القابلة للزراعة في جسم الإنسان. وتدعم المجسّات في الشبكة وظائف مختلفة؛ مثل مراقبة الجلكوز وقياس الإجهاد في العظام. وتعمل هذه المجسات بوجود رافعة مركزية متصلة بمستقبل خارج الجسم. والجدير بالذكر أن وجود رابط اتصال موثوق بين هذه المجسات أمر أساسي.

في هذه الورقة، تم تقدير فقد المسار بين هوائياتٍ حَلقية بيضوية ودائرية في العضلات وعظمين مختلفين هما: عظم العَضُد وعظم الفخذ، عند تردد مقداره 403 ميجاهيرتز. واتضح أن فقد المسار بين العضلات وعظم العَضُد أكبر بمقدار 33 ديسيبل من فقد المسار بين العضلات وعظم الفخذ. وعليه، يمكن بناء رابطٍ معياري يعمل بتعديلٍ قائم على ترميز إزاحة الطور (PSK) بصورة مثالية، فقط من عظم الفخذ إلى العضلة الواقعة فوق الوِرك.

وتشكل النتائج التي تم الحصول عليها في هذا البحث مصدراً جيداً للبيانات لحسابات ميزانيات الروابط في تطبيقات زراعة العظم.

Jordanian Journal of Computers and Information Technology (JJCIT), Vol. 04, No. 02, August 2018.

TOWARD AN ARABIC QUESTION ANSWERING SYSTEM OVER LINKED DATA

Abdelghani Bouziane[1], Djelloul Bouchiha[1], Noureddine Doumi[2] and Mimoun Malki[3]

(Received: 31-Dec.-2017, Revised: 21-Mar.-2018 and 09-Apr.-2018, Accepted: 15-Apr.-2018)

ABSTRACT

The increasing interest in Arabic natural language processing and semantic Web research involves an emerging need to the development of new Question Answering Systems (QAS). These systems allow users to ask a question in Arabic natural language and get the relevant answer. However, most existing QA systems focused on English and Latin-based languages. Less effort has been concentrated on the Arabic language, which belongs to "Semitic Languages". This work is an early version of a new domain-independent Arabic question answering system over linked data, which aims to particularly help Arab users to explore the Arabic Semantic Web based on Arabic ontology. We describe with sufficient details the different modules of our proposed system, which uses language parser, finite state automaton and semantic Web techniques to linguistically process and answer Arabic natural language question. Experiments have been carried out to evaluate and show efficiency of the proposed system.

KEYWORDS

Question answering system, Natural language processing (NLP), Linked data, Arabic language, Semantic Web, Ontology, SPARQL.

1. INTRODUCTION

Arabic is the most spoken language in the Semitic group and the official or co-official language of 26 countries, spoken by more than 422 million people in the Middle East and North Africa. Arabic is the fourth top language in the internet with 185 million users [1]. 54% of Google searches in the Middle East and North Africa (MENA) are now made in Arabic, 34% in English and 8% in French [2].

This accumulation of Arabic information on the Web, available in large quantities and in various formats, includes structured and unstructured data. This large amount of data must be accessible and controlled by users who want to access and manipulate this information. So, more sophisticated systems are needed. For this need, the existing search tools, like search engines and query languages, make finding information a complex and expensive task in terms of time. This difficulty has motivated the development of new adapted search tools; namely, Question Answering Systems (QAS), which allow users to ask a question in natural language and get the relevant answer.

Currently, mutation of these systems to the Web of data seems necessary to find the correct and accurate answers to users' questions. New question answering systems have to deal with Linked Data instead of the Web of documents. The Linked Data initiative aims at publishing structured and interlinked data on the Web by using Semantic Web technologies [3]. These technologies provide different languages for expressing data as graphs (RDF) and querying it (SPARQL) [4].

Despite the considerable research in question answering systems over semantic Web for English language, the development of Arabic QA systems over semantic Web is at its nascent stage. Due to the limits of Arabic NLP technologies [5] in Arabic Semantic Web, there are few works in the field of Arabic QAS over semantic Web and ontology [6]. Motivated by this challenge, we present in this paper an Arabic question answering system over linked data. The main objective of our system is to provide exact answers for Arabic natural language factoid questions, asked by native users, who don't know the complicated SPARQL query language. First, the proposed system receives as input an

1. A. Bouziane and D. Bouchiha are with EEDIS Lab., Ctr. Univ. Naama, Inst. Sciences and Technologies, Dept. Mathematics and Computer Science, Algeria. Emails: abdelghani.bouziane@univ-sba.dz and djelloul.bouchiha@univ-sba.dz
2. N. Doumi is with University of Saida, Dept. of Computer Science, Algeria. Email: noureddine.doumi@univ-saida.dz
3. M. Malki is with Lab RI- Sidi Bel-Abbes Ecole Supérieure en Informatique de Sidi Bel-abbes, Algeria. Email: m.malki@esi-sba.dz

Arabic natural language question, from which it provides the resource and keywords to the first module. Then, it uses a general SPARQL query to explore the ontology and gives the exact predicate by matching terms between keywords and predicates. Finally, our system provides an answer to the user question by running a final appropriate SPARQL query.

The rest of the paper is organized as follows. Section 2 highlights the challenge of the development of Arabic question answering systems over semantic Web. Section 3 reviews the existing related work. Section 4 presents the architecture of our proposed system. An illustrative example is covered in Section 5. Section 6 evaluates the resource extraction method, the stop-words' removal algorithm and the overall system accuracy. Finally, we summarize the paper and highlight the future work directions in Section 7.

2. MOTIVATION AND CHALLENGE

In this study, we present an Arabic natural language question answering system over semantic Web. The issue of developing such a system for poor resources in Arabic NLP [7] and Arabic Semantic Web is very challenging. Let's discuss in the following part of this section the difficulties in Arabic NLP and Arabic Semantic Web to highlight the development of Arabic question answering systems over semantic Web.

Arabic language is characterized by a relatively complex morphology. It has a rich system of morphological inflection. Arabic has also a high degree of ambiguity resulting from its diacritic-optional writing system, common deviation from spelling standards and absence of capital letters [8]. The existing tools and resources deal mainly with the Modern Standard Arabic (MSA), but the Arab World uses different Arabic dialects such as: (Egyptian Arabic (EGY), Levantine (LEV), Gulf Arabic (GLF), North African (Maghrebi) Arabic (Mag), Iraqi Arabic (IRQ), Yemenite Arabic (Yem)) [9]. There are limited resources and tools for Arabic language processing compared to English language. The other difficulty is the lack of Arabic support for Arabic language in the semantic Web technologies. The Arabic Semantic Web is very far from the best performance compared to English semantic Web. The difficulties of Arabic natural language processing hinder the development of Arabic Semantic Web, because the NLP is an important component of the semantic Web [10].

Another important component of the semantic Web is the Arabic ontology [11], which is said to be the foundation of the creation of Arabic Semantic Web designs. Recently, several works have dealt with the semantic Web for the Arabic language [11]-[12]. As can be seen from Table 1, there is weakness in ontology management tools for the Arabic language. So, there is a need to develop controlled vocabulary and ontology management tools for Arabic ontology for the foundation of Arabic Semantic Web [13].

Table 1. Examples of semantic web tools and their support to the Arabic language [13].

Tool	Arabic RDF ontology	Arabic OWL ontology	Arabic Query	Description
Protege	Support	Limited support	Limited support	Ontology editor
Jena	Support	Support	Limited support	Reasoner and processors
Sesame	Limited support	Limited support	No support	RDF database
KAON2	No support	No support	No support	Reasoner and ontology management

Table 1 shows how much some semantic Web tools support the Arabic language. The first column of Table 1 corresponds to the tool name. The columns "Arabic RDF ontology" and "Arabic OWL Ontology" indicate whether the tool supports these two languages (RDF and OWL) to express an Arabic ontology. The column "Arabic Query" indicates whether the tool allows interrogating the Arabic ontology with Arabic question. The "Description" column indicates the tool function.

3. RELATED WORK

The first survey of question answering systems backs to 1965, in which several systems were reviewed for the English language during the previous five years [14]. One of the first subtasks of question

answering systems is the Natural Language Interfacing to Data Bases (NLIDB), such as BASEBALL [15], PARRY [16], LUNAR [17] and NLWIDB [18]. Research in QA received a big surge in interest when a shared task on factoid QA was included in the 8th Text REtrieval Conference (TREC) [19]. Most systems process textual information, such as Youzheng et al. [20], Mulder [21], PALANTIR [22], QALC [23], Gómez et al. [24], Ryu et al. [25]. These question answering systems can be divided into three main distinct subtasks [26]-[28], which are Question Analysis, Document Retrieval and Answer Extraction. Most question answering systems follow these three subtasks. However, in the last years, the mutation of these systems to the Web of data seems necessary to find the correct and accurate answers to questions. New question answering systems have to deal with Linked Data instead of the Web of documents. Several systems appeared, such as AquaLog [28], SWIP [29], Xser [30], DeepQA IBM Watson's system [31] and E-librarian [32].

In the field of question answering systems for Arabic language, the situation is less bright. Research in this field is slow and gives limited results for all subtasks of QAS due to the lack of resources and tools in Arabic NLP [6]. Next are given works on Arabic QAS.

In [33], the authors proposed a question analysis for Arabic question answering systems using Stanford POS Tagger & parser for Arabic language, named entity recognizer, tokenizer, Stop-word removal, Question expansion, Question classification and Question focus extraction components to retrieve and extract the correct answer.

Al-Bayan [34] is a Question answering system for the holy Quran. The user asks Arabic natural language questions about the Quran. The system first retrieves the most relevant Quran verses. Second, it extracts the passage that contains the answer from two sources; the Quran and its interpretation books (Tafseer).

AQuASys [35] is designed to answer Arabic fact-based questions. It is composed of three modules: a question analysis module, a sentence filtering module and an answer extraction module.

In [36], the information source of the system is a given corpus or the Web pages. It uses supervised support vector machine (SVM) classifier for question classification and answer selection, to generate the exact answer for a given question in Arabic natural language.

AR2SPARQL [37] is an Arabic natural language interface for semantic Web, which uses linguistic and semantic analysis to convert the Arabic query into RDF triples, which are then matched with ontology triples to retrieve an answer.

AQAS [38] extracts answers from structured data. It is the first system of its type for the Arabic language. Knowledge from the radiation domain is presented using the frame technique. There is no published evaluation about AQAS.

QARAB [39]; [51] is an unconnected (non-Web-based) QA system for only factoid questions. No other type of question is supported. It uses IR and NLP techniques to extract answers from a collection of Arabic newspaper texts.

In [40], the authors use tagging rules and question patterns to analyze and understand an Arabic question in Arabic question answering environment.

ArabicQA [41] is an Arabic question answering system based on a Passage Retrieval (PR) module, a Named Entities Recognition (NER) module and an answer extraction module for Arabic texts.

In [42], the author describes a way to access Arabic Web Question Answering (QA) corpus using a chatbot (ALICE open-source chatbot initiative). ALICE is the Artificial Linguistic Internet Computer Entity. The system uses a simple (but large) set of pattern-template matching rules and converts a text corpus into the AIML chatbot model format.

In [43], the authors use lexical pattern for defining questions to extract the focus and Wikipedia article infoboxes, to generate cooperative answers for user-definitional questions. This approach can be integrated in all question answering systems.

The following table summarizes related works according to four criteria: (1) "Target source" indicates the name and type of the analyzed data, (2) "Question analysis techniques" correspond to the used analysis techniques by the considered system, (3) "Question classification techniques" correspond to

the used classification techniques and (4) "Performance", which gives some experimental results.

Table 2. Some Arabic QAS features and techniques.

System	Target source	Question analysis techniques	Question classification techniques	System Performance
Al bayan [34]	Quran and interpretation books (unstructured)	NLP technique	SVM classifier	Experts evaluation results: 0.73%
AQuASys [35]	Documents (unstructured)	Defined question structures and NLP technique	Defined question types and forms	Precision: 66.25 % Recall: 97.5%
AQAS [38]	Knowledge bases radiation diseases domain (structured)	Parser: morphological analysis	No	Not mentioned
QARAB [51]	Al-Raya Arabic newspaper text (unstructured)	NLP technique	Using a set of known question type	Precision: 97.3% Recall: 97.3%
WAHEED [36]	Web of document (unstructured)	NLP technique	SVM classifier	Mean Reciprocal Rank (MRR) : 65%
AR2SPARQL [37]	Ontology (structured)	NLP technique	No	Precision: 85.24% Recall: 61.61% F-measure: 71.5%
Al-Shawakfa [40]	Corpora of documents (unstructured)	NLP technique	Defined question type	Accuracy: 78.15% Recall: 97% F-measure: 86.56%
ArabicQA [41]	Set of documents (unstructured)	NLP technique	Defined question type	Not mentioned
Abu shawar [42]	Text corpus (unstructured)	Pattern-template matching rules	No	Recall: 93%
DefArabicQA [43]	Wikipedia article (semi-structured)	Lexical pattern	No	Accuracy: 63%

Most of works in Arabic question answering systems deal with unstructured data. Currently, with the growth of linked data technologies, new systems must interact with linked data instead of the Web of documents. Our proposed system tries to address these challenges by proposing a new solution that helps answer questions in Arabic natural language by translating them into SPARQL queries. In the next section, we describe the architecture of our proposed system.

4. PROPOSED SYSTEM

We propose an Arabic question answering system that transforms Arabic factoid questions into SPARQL query and then provides an exact answer drawn from an Arabic ontology-based knowledge base. Our proposed system accepts the Arabic simple factoid questions which may be in the following format (من هو\man. huw~a*who is*, من هي\man. hiy~a*who is*, ما هو\maA huw~a*what is*, ما هي\maA hiy~a*what is*, متى\mataý\when, مما\mim~aA*from what*, أين\Âay.na*where*, كيف\kay.fa*how*, في أي\fiy Âay~u*in what*, كم\kam.*how many*, بأي\biÂay~i*in what* …).

First, through its interface, the system receives the question in NL, processes it and finally produces an answer after formulating a SPARQL query that can be executed on Arabic Semantic Web, based on Arabic ontology. The transformation process is composed of three consecutive modules. Each one is composed of multiple steps depicted as presented in Figure 1. It starts with question processing. Then, predicate recognition is done. Finally, SPARQL query is formulated and executed.

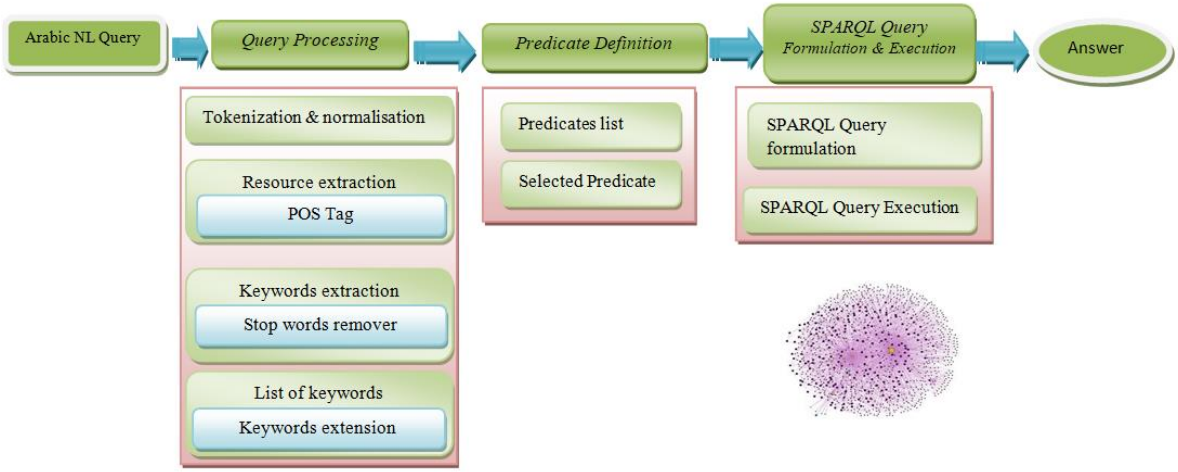

Figure 1. Architecture of the proposed system.

In the next sub-sections, we explain the above mentioned modules.

4.1 Question Processing Module

It is an important and crucial module. It allows analyzing an input natural language question, in order to have its constituents. This module has a big impact on the accuracy and the performance of any QA system. In our proposed system, the input question is linguistically processed and analyzed by the Question processing module, which consists of four steps: Tokenization and Normalization, Resource Extraction, Keywords Extraction and getting Keywords List. As a result, it provides the keywords list and the resources (named entities).

4.1.1 Tokenization and Normalization

The common step in NLP is Tokenization, which denotes the segmentation of the natural language text (question in our case) into individual consecutive basic units. A step of word normalization is necessary to reduce the spelling errors. These errors appear because the Arabic letter can be written in different styles. The correction of the most common spelling errors involves normalization of Arabic Alif 'ا' and Ya 'ي' characters [9]. We use MADAMIRA tools for the Tokenization and Normalization step [8].

Example: The Tokenization and Normalization step of the Arabic natural language question: ما هي عاصمه ألجزائر؟\maA hiy çaASimah ÂljazaAŷir ?*what is the capital of Algeria* ? provides "ما، هي، عاصمة، الجزائر". It normalizes the Alf 'ا'and Taa 'ة' in the words of this NL question.

Note that in this example and in the rest of this paper, every time we give an Arabic text and for readability purposes, we follow it with its HSB transliteration [44] and English translation for readability purposes.

4.1.2 Resource Extraction

The named entity is very important in most question answering systems for structured or unstructured data [45]. To date, as per to our knowledge, there are no Arabic Named Entity Recognition (NER) systems available for free. So, to gap this difficulty, we implemented our own NER. In our system, the named entity in the input question is the target resource to be explored for getting the correct answer. So, the Resource Extraction process consists of extracting the last Nominal Phrase (NP) of the Arabic question from the parse tree of the considered question. We use the Stanford Part-Of-Speech Tagger (pos-tagg) which is a Java implementation designed to provide a simple description of the grammatical relationships in a sentence [46].

Example: The last NP of the question ما هي عاصمة الجزائر؟\maA hiy çaASimaħu AljazaAŷir ?\ is the named entity الجزائر\AljazaAŷir*Algeria* in Figure 2.

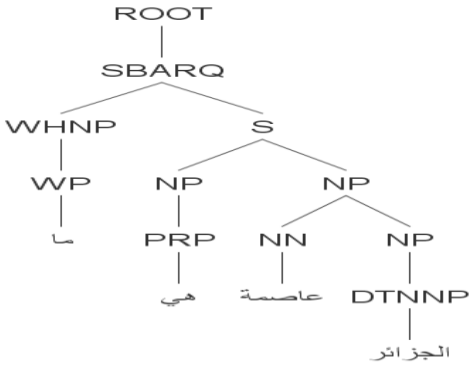

Figure 2. Parse tree of an Arabic question, given by Stanford POS Tagger.

4.1.3 Keywords Extraction

The keywords of the input question are used to generate the predicate of the <Subject, Predicate, Object> triple and to formulate the final SPARQL query.

To extract keywords from the input question, the system processes in two steps: First step is stop-words removal. Stop-words are the noisy words which frequently occur in the Arabic NL questions, such as prepositions, conjunctions and interrogative words. We propose a Finite State Automaton (FSA) that recognizes stop-words to be removed in our input Arabic question. The finite state automata technique (Figure 3) can accelerate the stop-words removing process [47].

In order to extract keywords, the second step consists of removing the words already recognized in the Resource Extraction step. Keywords are words that are not removed.

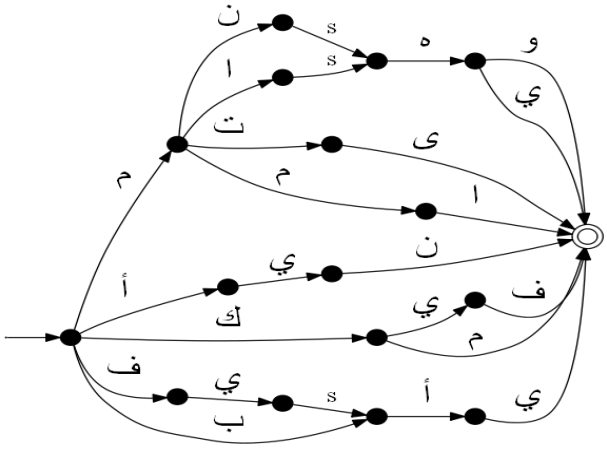

Figure 3. Stop-words finite sate automaton.

Example: From the text ما هي عاصمة الجزائر\maA hiy çaASimaħu AljazaAŷir*what is the capital of Algeria*, the stop-words removal gives ما هي \maA hiy*what is the*. Then the resource is الجزائر\AljazaAŷir*Algeria*. The rest عاصمة\çaASimaħu*capital* is the keyword of the question in natural language.

4.1.4 Keywords Extension

Keywords extracted in the previous step and the predicate used in the ontology may have a different morphology, but the same meaning. To gap this difficulty, we use Arabic WordNet [48, 49] to find synonyms, in order to extend the keywords set. These synonyms are morphologically normalized by the normalization process used in the first step of this module. A list of keywords is built to increase the probability to define the exact predicate in the next module.

4.2 Predicate Recognition

After the resource was fixed by the question processing module, the system uses a simple SPARQL

query to get all properties of our resource.

Question 1: ما هي عاصمة الجزائر؟\maA hiy ςaASimaħu AljazaAŷir*what is the capital of Algeria ?*

Question 2: متى ولد هواري بومدين؟ \matý wulida huwaAriy buwmad.yan*what is the birthday of Houari Boumedienne ?*

Resources of questions 1 and 2 are الجزائر\AljazaAŷir*Algeria* and هواري بومدين\huwaAriy buwmad.yan*Houari Boumedienne*, respectively. Now, we have to build a SPARQL query to retrieve the DBpedia Arabic properties of the resource in question:

Select ?p where{ < arabic-ontology-2#الجزائر > ?p ?o}
Select ?p where{ < arabic-ontology-2#هواري بومدين > ?p ?o}

The SPARQL resulting file is an XML document that is valid with respect to the XML Schema. The principal element is the SPARQL one. Inside the SPARQL element, there are two sub-elements: head and a result element. The result element contains the complete sequence of the query result. It has a child binding element. In this binding element, we find the query variable's name and value. We use the XQuery language to explore the XML document and build the predicate list.

Now, we match the keywords list with the predicates list. It is a lexical matching process, where the common word is selected to be the predicate.

4.3 SPARQL Query Formulation and Execution

Now, we are able to formulate the final SPARQL query with the resource and predicate to provide the exact answer from the Arabic ontology. For this, we use the template query:

Select ? Object where {Resource Property ?Object}

For the question ما هي عاصمة الجزائر؟\maA hiy ςaASimaħu AljazaAŷir ?*what is the capital of Algeria ?*, the SPARQL query is:

Select ? Object where {< arabic-ontology-2#الجزائر> *onto:* عاصمة *?Object}*

The result of the SPARQL query is an XML document, which will be parsed by the same process of the previous step to extract the correct answer.

5. ILLUSTRATIVE EXAMPLE

Now, we show a complete illustrative example of processing an Arabic natural language question. In this example, we assume that the introduced question to our system is:

من هو مؤلف رياض الصالحين؟\man huwa muŵlif riyaAD AlSAliHiyn?\, which corresponds to the English question *who is the author of The Meadows of the Righteous ?*

The question processing module takes place with 4 steps: Tokenization and Normalization, Resource Extraction, Keywords Extraction and Keywords List. Finally, it produces the following

Question: من هو مؤلف رياض الصالحين؟
Tokenization and Normalization: من, هو, مؤلف, رياض, الصالحين
Resource Extraction: the produced parse tree is (ROOT (SBARQ (WHNP (WP من)) (S (NP (PRP هو)) (NP (NN مؤلف) (NP (NNP رياض) (DTNNP الصالحين)))) (PUNC ?))). The resource is: رياض الصالحين
Keywords Extraction: first, the system eliminates the stop-words and the resource, so the keyword is: مؤلف
Keywords list: the system extends the keywords set by using Arabic WordNet, مؤلف\muŵalif\, كاتب\kaAtib\ *writer, author*.

The question processing module produces the following information to be the input of the next module.

Resource: رياض الصالحين\riyaAD AlSaAliHiyn*The Meadows of the Righteous*

List of keywords: مؤلف\muŵalif\, كاتب\kaAtib\ *writer, author*.

Predicate Recognition module: this module generates and executes the SPARQL query through the ontology to retrieve all predicates:

Select ?p where{ < arabic-ontology-2#رياض الصالحين > ?p ?o}

The result of the SPARQL query after processing is the predicate lists: اسم، مؤلف، لغة كتاب، بلد صدور\Ais.m, muŵalif, luγaħ kitaAb, baladu Suduwr*name, author, language of book, country of publication*.

Then, we select the predicate: مؤلف\ muŵalif*author* as a common term between the predicates list and the keywords list.

Finally, the system provides an XML document result by formulating and executing the SPARQL query:

SELECT ?object
WHERE {< semanticweb.org/ghani/ontologies/2017/6/untitled-ontology-2#رياض_الصالحين >
onto:مؤلف ?object }

The answer is extracted from the XML document:
يحيى_بن_شرف_النووي\yaH.yaý_b.nu_šaraf_Alnawawiy\

6. EVALUATION

Before evaluating the performance of our proposed system, it is important to briefly introduce the used dataset which is an Arabic ontology that we developed for this evaluation. The ontology depicted in Figure 4 covers notions surrounding the concept *Person*. An excerpt of the ontology shows the ontology classes (e.g. *Person*, *Occupation*, *Country* and *Place*), the object properties and the data type properties.

We carried out several experiments for a full evaluation of our system. We evaluated the performance of the Resource Extraction method, the Stop-words removal algorithm and the overall system accuracy.

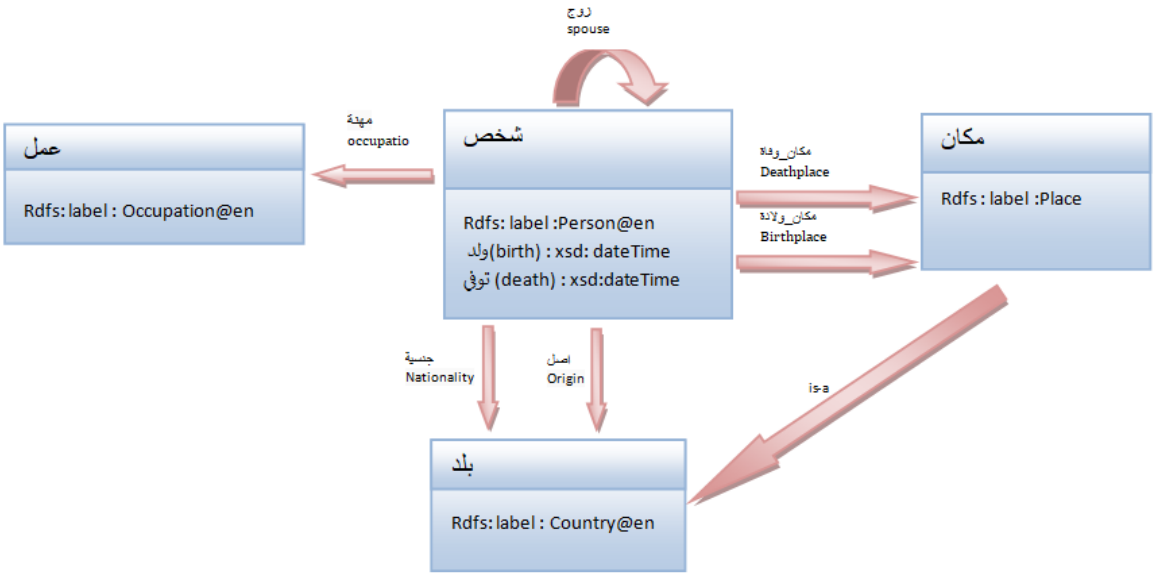

Figure 4. Excerpt of the ontology person.

For evaluating the resource extraction, the stop words removal and the overall system, we use a set of 50 factoid simple questions of different types about the ontology *Person*. This dataset is collected from the test-bed of the passage retrieval and question answering tasks proposed by Yassine Benajiba [50].

6.1 Evaluation Metrics

To measure the performance of our Resource Extraction, Stop-words Removal algorithm and the over-

all system, we used the following metrics: Precision, Recall and F-measure.

Precision (P) assesses the accuracy and is defined as follows:

Resource extraction process:

$$\text{Precision} = \frac{\text{number of correctely identified ressources}}{\text{total number of resources generated by the system}}$$

Stop words removal algorithm:

$$\text{Precision} = \frac{\text{number of correctely identified stop words}}{\text{total number of stop words generated by the system}}$$

System:

$$\text{Precision} = \frac{\text{number of correctely answered questions}}{\text{total number of questions answered by the system}}$$

The Recall (R) assesses the coverage and is defined as follows:

Resource extraction process:

$$\text{Recall} = \frac{\text{number of correctely identified ressources}}{\text{total number of resources}}$$

Stop-words removal algorithm:

$$\text{Recall} = \frac{\text{number of correctely identified stop words}}{\text{total number of stop words}}$$

System:

$$\text{Recall} = \frac{\text{number of correctely answered questions}}{\text{total number of introduced questions}}$$

Finally, F-measure is the trade-off, calculated by multiplying 2 times the product of Precision and Recall, divided by the sum of Precision and Recall. Mathematically, the F-measure formula is:

F-measure = 2 * (P*R) / (P+R).

6.2 Results and Discussion

In fact, the evaluations for the Resource Extraction, Stop-Words Removal algorithm and the overall system have been performed using dataset of [50]. The evaluation results are depicted in Table 3.

Table 3. Evaluation results, expressed in precision, recall and F-measure.

	Resource Extraction			Stop-Words Removal			System		
Number of questions	**Precision**	**Recall**	**F-measure**	**Precision**	**Recall**	**F-measure**	**Precision**	**Recall**	**F-measure**
05	1	1	1	1	1	1	1	1	1
10	0,8	0,88	0,83	0,9	0,95	0,92	0,8	0,8	0,8
15	0,8	0,85	0,82	0,93	0,95	0,94	0,78	0,73	0,75
20	0,75	0,83	0,78	0,9	0,95	0,92	0,77	0,7	0,73
30	0,73	0,7	0,71	0,95	0,95	0,95	0,71	0,66	0,68
40	0,73	0,71	0,71	0,95	0,95	0,95	0,7	0,67	0,68
50	0,73	0,71	0,71	0,96	0,96	0,95	0,71	0,69	0,7

6.2.1 Resource Extraction

For the Resource Extraction process, the resulting Precision, Recall and F-measure start respectively from 0.73, 0.70 and 0.71 to 1, as shown in Table 3. Precision and Recall need improvement, which reflects the need to add grammar rules and gazetteers into the Recognition process. The failure cases can be explained mainly by the incorrect parsing of some Arabic questions. The Arabic resources, which are Arabic names, are often in the form of nominal phrases, which consist of a noun stem or an

adjective with nominal reference. In some cases, Arabic nouns are more complicated and consist of more than one nominal phrases or verbal phrases.

6.2.2 Stop-words Removal

Using our question dataset, the accuracy of the Stop-words Removal algorithm is illustrated in Table 3. The resulting Precision, Recall and F-measure for the entire 30 simple factoid questions are high (0.95), which projects high accuracy.

6.2.3 System

As can be seen in Table 3, the system achieves successfully an average of 0.66 in terms of Recall and 0.71 in terms of Precision. The most likely explanations of the failure results of our system are the following:

- Resource Extraction failure: The previous evaluation results showed that the Resource Extraction process has a limited result, which affects negatively the accuracy of the system as can be seen in Figure 5.

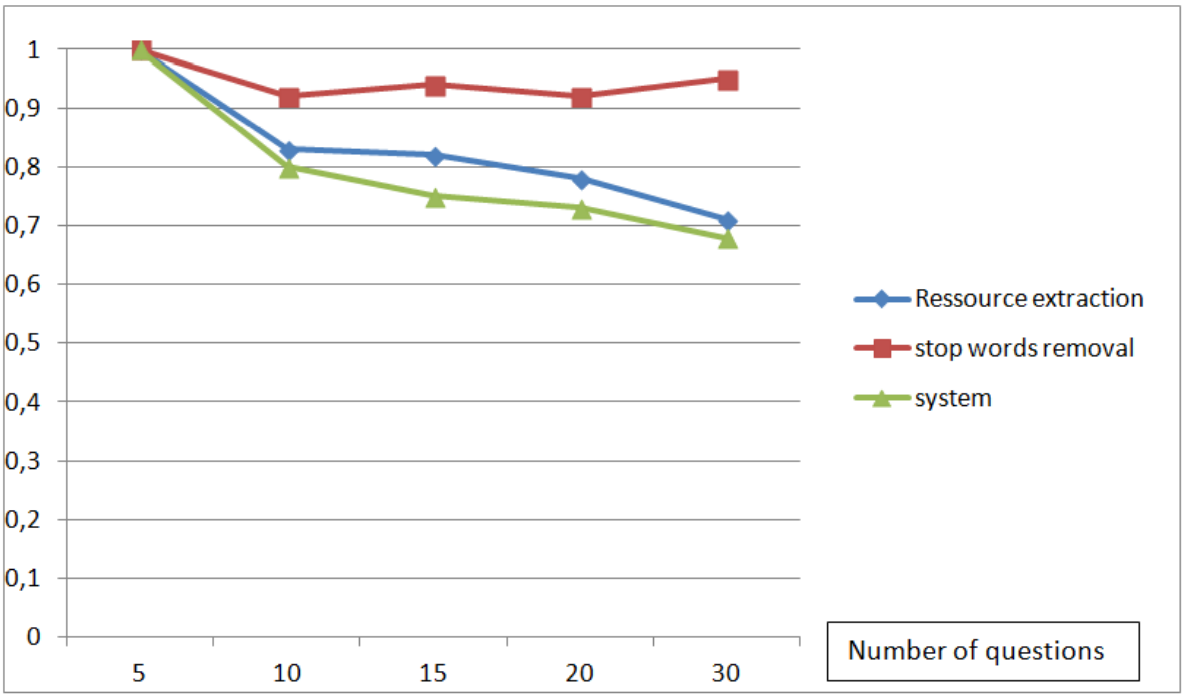

Figure 5. F-measure evaluation curves.

- Keywords failure: occurred when words could not be matched to any predicate of the appropriate resource. The most frequent causes of this type of errors can be classified into three main categories:
  - Recognition failure: this failure can occur when the user asks an Arabic question in unordinary and not standardized manner. Don't forget that our system deals with Modern Standardized Arabic (MSA) questions. The main cause of the Recognition failure can be explained by the Resource Extraction failure and the Stop-Words Removal failure.
  - Extension failure: occurs when the system doesn't generate any synonym of the predicate using the Arabic WordNet resource.
  - Matching failure: occurs when the list of keywords can't be matched to any predicate. So, the vocabulary of the ontology must use the most frequent words.

7. CONCLUSION AND FUTURE WORKS

We presented a question answering system that provides answers to questions expressed in Arabic natural language. We believe that the proposed system makes a step towards enabling users to explore the growing Arabic content on the Semantic Web. The system uses techniques from NLP and semantic Web to process the input question and to transform it into SPARQL query to get answers from Arabic Semantic Web based on ontology. First, the system applies a linguistic process to the input question in order to provide the resource and a list of keywords. Second, all the predicates of the resource are selected and matched to the keyword list in order to identify the appropriate predicate which form the <Resource, Predicate, Object> triple. Finally, our system formulates and executes a final SPARQL query to get an exact answer.

We discussed the major challenges of developing this kind of system for Arabic language, which is valuable for further study in more depth. Based on the evaluation results, it can be concluded that this research field is very promising. However, we plan to resolve some of the limitations we found in our evaluation by improving the existing modules using natural language processing techniques, as well as other tools and resources.

Since this is one of the first works aiming Arabic question answering system over linked data, there are many directions to extend our work. First is to add new modules such as question categorization. Second is to extend this work to cover other complex cases in Arabic question. Finally, is to apply our proposed approach to a real-world example of the Arabic DBpedia chapter, which is the real world example of the Arabic Semantic Web provided by the DBpedia community.

REFERENCES

[1] M. M. Goup, Internet World Users By Language: Top 10 Languages, [Online], Available: http://www.internetworldstats.com/stats7.htm, [Accessed October 2017].

[2] B. v. d. Beld, State of Digital, The Arabic Web: Numbers and Facts, General Statistics, [Online], Available: http://www.stateofdigital.com/the-arabic-web/, [Accessed October 2017].

[3] S. Albagli, R. Ben-Eliyahu-Zohary and S. E. Shimony, "Markov Network-based Ontology Matching," Journal of Computer and System Sciences, vol. 78, pp. 105-118, 2012.

[4] P. Hitzler, M. Krotzsch and S. Rudolph, Foundations of Semantic Web Technologies: CRC Press, 2009.

[5] W. Zaghouani, "Critical Survey of the Freely Available Arabic Corpora," arXiv Preprint arXiv:1702.07835, 2017.

[6] A. Bouziane, D. Bouchiha, N. Doumi and M. Malki, "Question Answering Systems: The Story Till the Arabic Linked Data," International Journal of Artificial Intelligence and Soft Computing (IJAISC), vol. 6, pp. 24-42, 2017.

[7] A. M. Ezzeldin and M. Shaheen, "A Survey of Arabic Question Answering: Challenges, Tasks, Approaches, Tools and Future Trends," Proceedings of The 13th International Arab Conference on Information Technology (ACIT 2012), pp. 1-8, 2012.

[8] A. Pasha, M. Al-Badrashiny, M. Diab, A. E. Kholy, R. Eskander, N. Habash, M. Pooleery, O. Rambow and R. M. Roth, "MADAMIRA: A Fast, Comprehensive Tool for Morphological Analysis and Disambiguation of Arabic," Ed. LREC2014, 2014.

[9] N. Habash, Introduction to Arabic Natural Language Processing: Morgan & Claypool, 2010.

[10] R. Guo and F. Ren, "Towards the Relationship Between Semantic Web and NLP," International Conference on Natural Language Processing and Knowledge Engineering, Dalian, 2009.

[11] M. M. Boudabous, L. H. Belguith and F. Sadat, "Exploiting the Arabic Wikipedia for Semi-automatic Construction of a Lexical Ontology," International Journal of Metadata, Semantics and Ontologies, vol. 8, pp. 245-253, 2013.

[12] H. Al-Feel, "The Roadmap for the Arabic Chapter of DBpedia," Mathematical and Computational Methods in Electrical Engineering, Proceedings of the 14th International Conference on Telecom. and Informatics (TELE-INFO '15), Sliema, Malta, pp. 115-125, 2015.

[13] M. Beseiso, A. R. Ahmad and R. Ismail, "A Survey of Arabic Language Support in Semantic Web," International Journal of Computer Applications, vol. 9, pp. 35-40, 2010.

[14] R. F. Simmons, "Answering English Questions by Computer: A Survey," Communications of the ACM, vol. 8, pp. 53-70, 1965.

[15] B. F. Green, A. K. Wolf, C. Chomsky and K. Laughery, "BASEBALL: An Automatic Question Answering," Proceedings of Western Joint Computer Conference, pp. 207-216, 1961.

[16] K. M. Colby, "Artificial Paranoia," Artificial Intelligence, vol. Vol. 2, 1971.

[17] W. Woods, R. Kaplan and B. Webber, "The Lunar Sciences Natural Language Information System," Cambridge, Massachusetts Final Report, 1972.

[18] A. Rukshan, R. Prashanthi and M. Sinnathamby, "Natural Language Web Interface for Database (NLWIDB)," Proceedings of the 3rd International Symposium, SEUSL, Oluvil, Sri Lanka, 2013.

[19] E. M. Voorhees and D. M. Tice, "The TREC-8 Question Answering Track Evaluation," NIST Special Publication 500-246: The 8th Text REtrieval Conference (TREC 8), 1999.

[20] W. Youzheng, H. Chiori, K. Hideki and K. Hisashi, "Leveraging Social Q&A Collections for Improving Complex Question Answering," Elsevier, Computer Speech and Language, vol. 29, pp. 1-19, 2015.

[21] C. Kwok, O. Etzioni and D. Weld, "Scaling Question Answering to the Web," Proceedings of the 10th International Conference on World Wide Web, Hong Kong, China, pp. 150-161, 2001.

[22] S. Harabagiu Dan, A. Harabagiu, D. Moldovan, C. Clark, M. Bowden, A. Hickl and P. Wang, "Employing Two Question Answering Systems in TREC 2005," Proceedings of the 14th Text REtrieval Conference, 2005.

[23] O. Ferret, B. Grau, G. Illouz, C. Jacquemin and N. Masson, "QALC - The Question-Answering Program of the Language and Cognition Group at LIMSI-CNRS," TREC-8, Columbia, 1999.

[24] J. M. G. Soriano, M. M. Y. Gómez, E. S. Arnal and P. Rosso, "A Passage Retrieval System for Multilingual Question Answering," International Conference on Text, Speech and Dialogue, pp. 443-450, 2005.

[25] P.-M. Ryu, M.-G. Jang and H.-K. Kim, "Open Domain Question Answering Using Wikipedia-based Knowledge Model," Information Processing & Management, vol. 50, pp. 683-692, 2014.

[26] R. Sutcliffe, A. Peñas, E. Hovy, P. Forner, Á. Rodrigo, C. Forascu, Y. Benajiba and P. Osenova, "Overview of QA4MRE Main Task at CLEF 2013," Working Notes CLEF, 2013.

[27] S. K. Ray and K. Shaalan, "A Review and Future Perspectives of Arabic Question Answering Systems," IEEE Transactions on Knowledge and Data Engineering, vol. 28, pp. 3169-3190, 2016.

[28] V. Lopez, V. Uren, M. Sabou and E. Motta, "Is Question Answering Fit for the Semantic Web? A Survey, " Semantic Web, vol. 2, pp. 125–155, 2011.

[29] C. Pradel, O. Haemmerlé and N. Hernandez, "Swip: A Natural Language to SPARQL Interface Implemented with SPARQL," 21st International Conference on Conceptual Structures (ICCS 2014), Iaşi, Romania, 2014.

[30] K. Xu, S. Zhang, Y. Feng and D. Zhao, "Answering Natural Language Questions *via* Phrasal Semantic Parsing," The Natural Language Processing and Chinese Computing, Third CCF Conference (NLPCC 2014), Shenzhen, China, 2014.

[31] A. Kalyanpur, B. K. Boguraev, S. Patwardhan, J. W. Murdock, A. Lally, C. Welty, J. M. Prager, B. Coppola, A. Fokoue-Nkoutche, L. Zhang, Y. Pan and Z. M. Qiu, "Structured Data and Inference in DeepQA," IBM Journal of Research and Development, vol. 56, pp. 10:1 - 10:14, May-June 2012.

[32] S. Linckels and C. Meinel, "A Simple Solution for an Intelligent Librarian System," Proceedings of the IADIS International Conference of Applied Computing (IADIS AC2005), Lisbon, Portugal, pp. 495-503, 2005.

[33] W. Ahmed and A. P. Babu, "Question Analysis for Arabic Question Answering Systems," International Journal on Natural Language Computing (IJNLC), vol. 5, December 2016.

[34] H. Abdelnasser, R. Mohamed, M. Ragab, A. Mohamed, B. Farouk, N. El-Makky and M. Torki, "Al-Bayan: An Arabic Question Answering System for the Holy Quran," Proceedings of the EMNLP 2014 Workshop on Arabic Natural Langauge Processing (ANLP), Doha, Qatar, pp. 57–64, 2014.

[35] S. Bekhti and M. Al-Harbi, "AQuASys: A Question-Answering System for Arabic," Proceedings of the 13th International Conference on Applied Computer Science (ACS '13), Proceedings of the 2nd

International Conference on Digital Services, Internet and Applications (DSIA'13), Morioka City, Iwate, Japan, pp. 130-139, 2013.

[36] W. Ahmed, A. Pv and A. P. Babu, "Web-based Arabic Question Answering System using Machine Learning Approach," International Journal of Advanced Research in Computer Science, vol. 8, pp. 40-45, Jan./Feb. 2017.

[37] I. Al-Agha and A. Abu-Taha, "AR2SPARQL: An Arabic Natural Language Interface for the Semantic Web," International Journal of Computer Applications, vol. 125, 2015.

[38] F. A. Mohammed, K. Nasser and H. M. Harb, "A Knowledge-based Arabic Question Answering System (AQAS)," ACM SIGART Bulletin, vol. 4, pp. 21-30, Oct. 1993.

[39] B. Hammo, H. Abu-Salem and S. Lytinen, "QARAB: A Question Answering System to Support the Arabic Language," Proceedings of the ACL-02 Workshop on Computational Approaches to Semitic Languages (SEMITIC'02), Philadelphia, Pennsylvania, pp. 1-11, 2002.

[40] E. Al-Shawakfa, "A Rule-based Approach to Understand Questions in Arabic Question Answering," Jordanian Journal of Computers and Information Technology, vol. 2, pp. 210-231, 2016.

[41] Y. Benajiba, P. Rosso and A. Lyhyaoui, "Implementation of the ArabiQA Question Answering System's Components," Proc. Of Workshop on Arabic Natural Language Processing, 2nd Information Communication Technologies Int. Symposium (ICTIS-2007), Fez, Morroco, pp. 3-5, April, 2007.

[42] B. A. Shawar, "A Chatbot As a Natural Web Interface to Arabic Web QA," International Journal of Emerging Technologies in Learning (iJET), vol. 6, pp. 37-43, 2011.

[43] O. Trigui, L. H. Belguith and P. Rosso, "Arabic Cooperative Answer Generation via Wikipedia Article Infoboxes," Research in Computing Science, vol. 132, pp. 129-153, 2017.

[44] N. Y. Habash, A. Soudi and T. Buckwalter, "On Arabic Transliteration," Arabic Computational Morphology: Knowledge-based and Empirical Methods, vol. 38, A. Soudi, A. v. d. Bosch and G. Neumann, Eds., Springer, pp. 15-22, 2007.

[45] Y. Benajiba, M. Diab and P. Rosso, "Using Language -Independent and Language- Specific Features to Enhance Arabic Named Entity Recognition," The International Arab Journal of Information Technology, vol. 6, 2009.

[46] M. C. De Marneffe and C. D. Manning, Stanford Typed Dependencies Manual, Stanford University, Ed. 2008, pp. 338-345, Sep. 2008.

[47] R. Al-Shalabi, G. Kanaan, J. M. Jaam, A. Hasnah and E. Hilat, "Stop-word Removal Algorithm for Arabic Language," Proceedings of International Conference on Information and Communication Technologies: From Theory to Applications, Damascus, Syria, 2004.

[48] H. Rodríguez, D. Farwell, J. Farreres, M. Bertran, M. Alkhalifa, M. A. Martí, W. Black, S. Elkateb, J. Kirk, P. Vossen and C. Fellbaum, "Arabic WordNet: Current State and Future Extensions," Proceedings of the 4th Global WordNet Conference (GWC 2008), Szeged, Hungary, 2008.

[49] Y. Regragui, L. Abouenour, F. Krieche, K. Bouzoubaa and P. Rosso, "Arabic WordNet: New Content and New Applications," Proceedings of the 8th Global WordNet Conference, pp. 330-338, 2016.

[50] Y. Benajiba, "Test-Bed for Passage Retrieval (PR) and Question Answering (QUA) Tasks," Y. Benajiba, Ed., [Accessed October 2017].

[51] B. Hammo, S. Abuleil, S. Lytinen and M. Evens: "Experimenting with a Question Answering System for the Arabic Language," Computers and the Humanities, vol. 38, no. 4, pp. 397-415, 2004.

ملخص البحث:

يتضمن الاهتمام المتزايد بمعالجة نصوص اللغة العربية وبحوث الشبكة العنكبوتية في مجال دلالات الألفاظ وتطورها حاجةً إلى تطوير أنظمة جديدة للإجابة عن الأسئلة. وتسمح هذه الأنظمة للمستخدمين بطرح أسئلة باللغة العربية والحصول على إجاباتٍ لها.

وتجدر الإشارة إلى أن غالبية أنظمة الإجابة عن الأسئلة المتاحة على الشبكة تركز على اللغة الإنجليزية واللغات ذات الأصل اللاتيني، مع القليل من الجهد الذي يركز على اللغة العربية التي تندرج تحت مسمّى اللغات الساميّة.

والبحث الذي بين أيدينا نسخة مبكرة من نظام جديد للإجابة عن الأسئلة باللغة العربية باستخدام البيانات المرتبطة. والنظام المقترح يهدف إلى مساعدة المستخدمين العرب في استكشاف دلالات الألفاظ وتطورها على الشبكة العنكبوتية.

في هذا البحث، نصف بتفصيلٍ كافٍ الوحدات التي يتألف منها نظام الإجابة عن الأسئلة المقترح لمعالجة الأسئلة المطروحة باللغة العربية لغويّاً من أجل إيجاد الإجابات الصحيحة لها. وقد أجريت تجارب لتقييم النظام المقترح وبيان فاعليته.

Jordanian Journal of Computers and Information Technology (JJCIT), Vol. 04, No. 02, August 2018.

IMPROVED TESTABILITY METHOD FOR MESH-CONNECTED VLSI MULTIPROCESSORS

Jamil Al-Azzeh

(Received: 04-Feb.-2018, Revised: 27-Mar.-2018 and 16-Apr.-2018, Accepted: 25-Apr.-2018)

ABSTRACT

The problem of in-operation embedded hardware-level fault detection in mesh-connected VLSI multiprocessors is considered. A new approach to the multiprocessor test based on the mutual inter-unit checking is presented, which allows increasing the successful fault detection probability. Formal rules are defined for forming sets of testing and tested neighbors for each unit which are invariant to the location of the unit within the topological structure of the multiprocessor and its dimension. The final test result for each processor unit is formed by applying the majority operator to the individual faulty/healthy tags calculated by all testing neighbors. The formulae to determine the number of testing neighbors for each unit depending on the dimension of the multiprocessor are given. The successful fault detection probability is evaluated in the case when the proposed approach is used; the successful fault detection probability vs. multiprocessor dimension and the successful fault detection probability vs. the individual test unit reliability dependencies are investigated. The proposed approach is shown to provide increased successful fault detection probability compared to the self-test for all practically significant cases.

KEYWORDS

Mesh-connected VLSI multiprocessors, Fault tolerance, Testability, Built-in self-test, Mutual inter-unit test, Majority operator.

NOMENCLATURE

D	The number of dimensions in the multiprocessor mesh
$u_{x_1x_2\ldots x_d}$	A unit of a d-dimensional multiprocessor
x	The horizontal coordinate of a unit in the mesh
y	The vertical coordinate of a unit in the mesh
z	The "depth" coordinate of a unit in the 3D mesh
m	The number of rows in the multiprocessor mesh
n	The number of columns in the multiprocessor mesh
p	The "depth" of the 3D multiprocessor mesh
$C_{x_1x_2\ldots x_d}$	The set of neighbors tested by processor unit $u_{x_1x_2\ldots x_d}$
$K_{x_1x_2\ldots x_d}$	The set of neighbors testing processor unit $u_{x_1x_2\ldots x_d}$
$\varphi_{x_1x_2\ldots x_d}$	The faulty/non-faulty flag of processor unit $u_{x_1x_2\ldots x_d}$
$\varphi_{x_1x_2\ldots x_d}^{x'_1x'_2\ldots x'_d}$	The partial faulty/non-faulty flag of a tested processor unit $u_{x'_1x'_2\ldots x'_d}$ formed by testing processor unit $u_{x_1x_2\ldots x_d}$
$u_{x_1^ix_2^i\ldots x_d^i}$	An i^{th} tested neighbor of processor unit $u_{x_1x_2\ldots x_d}$

J. Al-Azzeh is with Department of Computer Engineering, Al-Balqa Applied University, Al-Salt, Jordan. Email: jamil.azzeh@bau.edu.jo

B_i	An i^{th} parallel thread of the mutual inter-unit test algorithm
$T^{x_1x_2\ldots x_d}(k)$	A k^{th} test signature produced by testing unit $u_{x_1x_2\ldots x_d}$
$k^{\max}_{x_1x_2\ldots x_d}$	The number of test signatures supported by testing unit $u_{x_1x_2\ldots x_d}$
$R^{x_1^i x_2^i \ldots x_d^i}(k)$	The test response signature issued by a tested unit $u_{x_1^i x_2^i \ldots x_d^i}$ after $T^{x_1x_2\ldots x_d}(k)$ is received
$R_0^{x_1^i x_2^i \ldots x_d^i}(k)$	The reference test response signature expected to be issued by a tested unit $u_{x_1^i x_2^i \ldots x_d^i}$ after receiving test signature $T^{x_1x_2\ldots x_d}(k)$
$\tau_0^{\max}$	The interval of time between two adjacent test loops
τ_0	Next test loop wait counter
$\tau_i^{\max}$	The maximum time needed to form the test response by an i^{th} tested unit $u_{x_1^i x_2^i \ldots x_d^i}$
τ_i	Test response wait counter
$\pi^+(t)$	The probability that a processor unit is properly detected as faulty by a separate test unit
$P^+(t)$	The probability that a processor unit is properly detected as faulty by a set of testing neighbors
C_j^i	The number of combinations of i elements out of j
#	The majority operator

1. INTRODUCTION

Many modern computer applications require the use of high performance VLSI-based embedded systems to attain desired efficiency, low cost and high flexibility [1]-[22]. VLSI multiprocessors (VLSI MPs), also known as multicore processors, represent a highly efficient solution for implementing such high performance embedded systems, combining fine-grain concurrency with decentralized and logically distributed architecture [23]. Increasing complexity of VLSI MPs becomes a problem, because the probability that a processor unit or a link in a multiprocessor may appear faulty (defective) grows relatively high as the number of processor units increases [24]-[25].

A VLSI multiprocessor containing defective units (and links) can be made healthy as a whole subject to dedicated defect detection and isolation mechanism is employed [26]-[27]. If a certain redundancy, e.g., a set of spare units is introduced and specific methods are used to make it possible to detect and logically replace defect units with spare ones, then the VLSI MP may be treated as defect-free and retains its performance at the same time. In both cases, a multiprocessor with physical defects is logically reconfigured and VLSI MP fabrication yield loss is reduced as a result.

For successful VLSI MP logical reconfiguration [26], it is important that every faulty node is properly detected and isolated to let the rest of the multiprocessor operate [27], possibly, with slightly decreased performance [28]. This problem is typically solved based on the usage of self-checking or self-test methods [29]-[41]. Self-test technique allows detecting both manufacturing defects and local faults and is a suitable solution to provide fast fault/defect detection that does not require powering off and un-mounting the multiprocessor for repair. However, relatively low testability is the main problem of the

self-test approach, because test hardware itself is not 100% reliable; yet, self-checking algorithms may miss many faults/defects and sometimes treat healthy units as defective. To significantly alleviate the above problem, mutual inter-unit test can be employed, meaning that each multiprocessor unit is checked by some other units and the final faulty/non-faulty decision is made based on a certain formal rule, which takes into account the local decisions made by particular test units [39]-[41]. This approach is developed in the present paper.

The aim of the manuscript is to expand the VLSI multiprocessor mutual inter-unit test method initially presented in [39]-[41]. In the following sections, we formally state the mutual inter-unit test approach for the d-dimensional VLSI MP architecture, which makes it possible to concurrently detect faulty/defective units across a mesh-connected VLSI multiprocessor. A parallel inter-unit test algorithm is presented based on the proposed formal approach and dedicated test hardware implementing the above algorithm is diagrammed and briefly discussed. At the end of the paper, we demonstrate that the mutual inter-unit test environment provides increased testability compared to the self-checking technique.

2. THE MUTUAL INTER-UNIT TEST APPROACH

The key idea of the mutual inter-unit test is that each processor unit of the multiprocessor is periodically checked by a subset of its physical neighbors (so called "testing neighbors") and, at the same time, this processor unit tests another subset of its physical neighbors (so called "tested neighbors") and the final faulty/non-faulty decision for each processor unit is made based on the majority operator result obtained from the partial results returned by the testing neighbors.

The set of "testing neighbors" for each processor unit is formed depending on the number of dimensions (d) of the VLSI multiprocessor topology and should satisfy the odd cardinality requirement to make the majority operator applicable to produce the final test result. The same applies to the formation of the set of "tested neighbors", except that the cardinality of the set may not be odd. The process of mutual inter-unit test is carried out simultaneously in all the units across the mesh, so that a faulty signal is simultaneously transferred to the physical neighbors of the corresponding faulty processor unit, which makes it possible to efficiently isolate (or replace) faulty/defective units in a timely manner.

The mutual inter-unit test mechanism may be considered as an advanced form of self-checking, because the operability of the test hardware itself is also tested. For example, if one of the testing processor units produces a wrong faulty/non-faulty decision, then the tested unit (which is in fact non-faulty) will not be necessarily detected as faulty by mistake as the resulting faulty signal is formed by the majority operator applied to a set of partial fault detection signals. This means that the mutual inter-unit test mechanism testability is better compared to the self-test technique. A more formal demonstration is shown at the end of the paper.

3. THE FORMATION OF TESTING AND TESTED NEIGHBOR SETS

The formation of testing and tested neighbor sets is one of the key problems in the organization of mutual inter-unit test. In this section, we provide formal rules to define these sets for a VLSI MP of arbitrary dimension $d \geq 2$.

Let us first consider a 2-dimensional multiprocessor. Let $U = \{u_{xy}\}$ be the set of its processor units, where x and y are coordinates (indices) of a particular unit in the mesh in the horizontal and vertical dimensions, respectively, $x = \overline{0, n-1}$, $y = \overline{0, m-1}$, with m and n standing for the number of rows and columns of the mesh, respectively. Let C_{xy} and K_{xy} designate the sets of tested and testing neighbors of processor unit u_{xy}, respectively. Then, for given arbitrary $x \in \{0,1, \dots n-1\}$ and $y = \{0,1, \dots m-1\}$, we can formulate the following rules:

$$C_{xy} = \left\{ \begin{array}{c} u_{(x+1) \bmod n, y}, \\ u_{(x+1) \bmod n, (y+1) \bmod m}, \\ u_{x, (y+1) \bmod m} \end{array} \right\} \quad (1)$$

$$K_{xy} = \begin{Bmatrix} u_{x,(y+(1-\text{sign}(y))m-1)}, \\ u_{(x+(1-\text{sign}(x))n-1),(y+(1-\text{sign}(y))m-1)}, \\ u_{(x+(1-\text{sign}(x))n-1),y} \end{Bmatrix} \quad (2)$$

Equations (1) and (2) above take into account the fact that leftmost, rightmost, topmost and bottommost processor units have fewer physical neighbors than those located in the other parts of the mesh. For example, a topmost unit has no neighbor above, that's why its tested neighbor set should include the bottommost unit in the same column. The same applies to a leftmost unit that has no neighbor on its left; its testing neighbor set should include the rightmost unit in the same row. Figure 1 illustrates rules (1) and (2) in detail. Note that rules (1) and (2) give just one of several possible testing/tested neighbor allocations around each unit, providing the minimal number of neighbors involved.

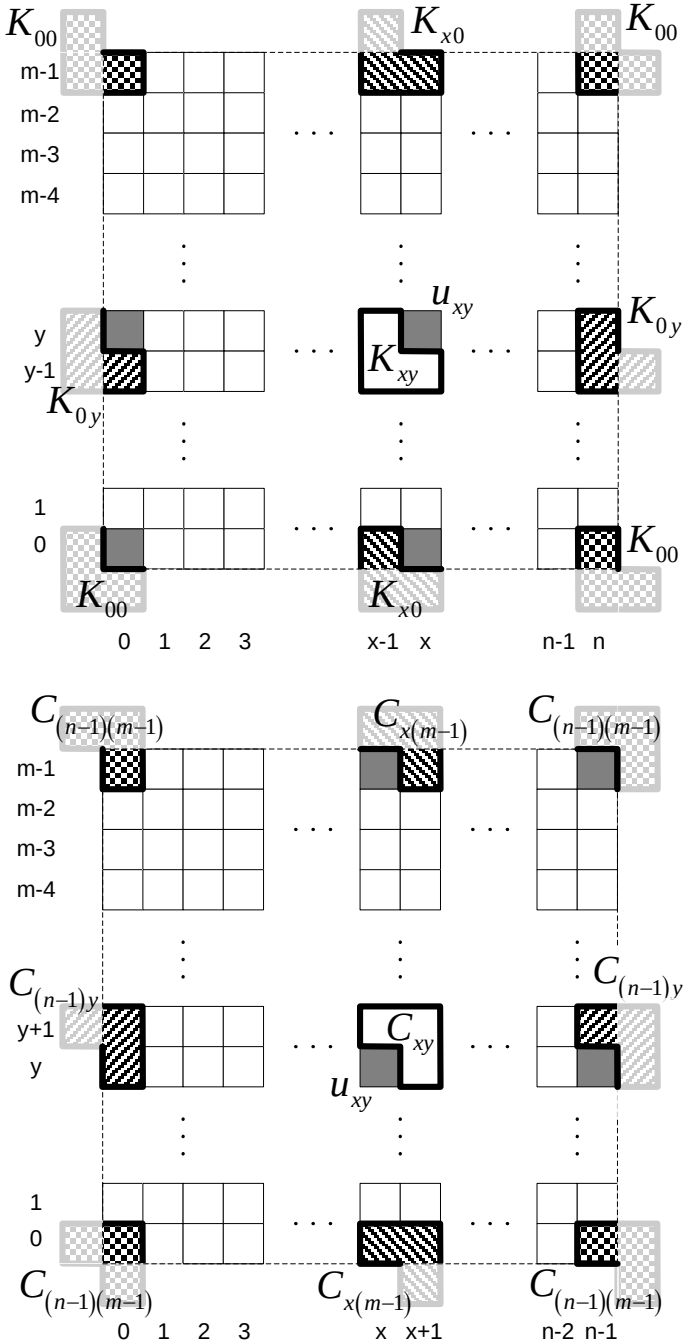

Figure 1. The formation of tested and testing neighbor sets in a 2-dimensional mesh multiprocessor.

If set K_{xy} is defined for each processor unit u_{xy} , then the faulty/non-faulty decision may be made according to the following rule:

$$\varphi_{xy} = \#\left\{ \begin{array}{c} \varphi_{xy}^{\left(x+(1-\mathrm{sign}(x))n-1\right),y}, \\ \varphi_{xy}^{\left(x+(1-\mathrm{sign}(x))n-1\right),\left(y+(1-\mathrm{sign}(y))m-1\right)}, \\ \varphi_{xy}^{x,\left(y+(1-\mathrm{sign}(y))m-1\right)} \end{array} \right. \tag{3}$$

where # denotes the majority operator, $\varphi_{xy}^{x'y'} = 1$, if unit u_{xy} 'is considered' non-faulty by unit $u_{x',y'}$ and $\varphi_{xy}^{x'y'} = 0$ otherwise, where x', y' are the placeholders standing for the corresponding upper indices in Equation (3). According to (3), unit u_{xy} is treated as faulty and needs to be isolated from the mesh, if $\varphi_{xy} = 0$.

The rules (1)-(3) may be easily extended to mesh topologies of higher dimensions. For example, for a 3-dimensional multiprocessor they could be formulated as follows:

$$C_{xyz} = \left\{ \begin{array}{c} u_{(x+1)\bmod n,y,z}, u_{x,(y+1)\bmod m,z}, \\ u_{x,y,(z+1)\bmod p}, u_{(x+1)\bmod n,(y+1)\bmod m,z}, \\ u_{(x+1)\bmod n,y,(z+1)\bmod p}, \\ u_{x,(y+1)\bmod m,(z+1)\bmod p}, \\ u_{(x+1)\bmod n,(y+1)\bmod m,(z+1)\bmod p} \end{array} \right\} \tag{4}$$

$$K_{xyz} = \left\{ \begin{array}{c} u_{\left(x+(1-\mathrm{sign}(x))n-1\right),y,z}, \\ u_{x,\left(y+(1-\mathrm{sign}(y))m-1\right),z}, \\ u_{x,y,\left(z+(1-\mathrm{sign}(z))p-1\right)}, \\ u_{\left(x+(1-\mathrm{sign}(x))n-1\right),\left(y+(1-\mathrm{sign}(y))m-1\right),z}, \\ u_{\left(x+(1-\mathrm{sign}(x))n-1\right),y,\left(z+(1-\mathrm{sign}(z))p-1\right)}, \\ u_{x,\left(y+(1-\mathrm{sign}(y))m-1\right),\left(z+(1-\mathrm{sign}(z))p-1\right)}, \\ u_{\left(x+(1-\mathrm{sign}(x))n-1\right),\left(y+(1-\mathrm{sign}(y))m-1\right),\left(z+(1-\mathrm{sign}(z))p-1\right)} \end{array} \right\} \tag{5}$$

$$\varphi_{xyz} = \#\left\{ \begin{array}{c} \varphi_{xy}^{\left(x+(1-\mathrm{sign}(x))n-1\right),y,z}, \\ \varphi_{xy}^{x,\left(y+(1-\mathrm{sign}(y))m-1\right),z}, \\ \varphi_{xy}^{x,y,\left(z+(1-\mathrm{sign}(z))p-1\right)}, \\ \varphi_{xy}^{\left(x+(1-\mathrm{sign}(x))n-1\right),\left(y+(1-\mathrm{sign}(y))m-1\right),z}, \\ \varphi_{xy}^{\left(x+(1-\mathrm{sign}(x))n-1\right),y,\left(z+(1-\mathrm{sign}(z))p-1\right)}, \\ \varphi_{xy}^{x,\left(y+(1-\mathrm{sign}(y))m-1\right),\left(z+(1-\mathrm{sign}(z))p-1\right)}, \\ \varphi_{xy}^{\left(x+(1-\mathrm{sign}(x))n-1\right),\left(y+(1-\mathrm{sign}(y))m-1\right),\left(z+(1-\mathrm{sign}(z))p-1\right)} \end{array} \right\} \tag{6}$$

where m, n and p are the sizes of the mesh in X, Y and Z dimensions, respectively. To define sets $C_{x_1x_2\ldots x_d}$ and $K_{x_1x_2\ldots x_d}$ for a general cased-dimension mesh, it is necessary to extend Equations (4)-(6) by adding extra properly indexed elements (u and φ) and all possible combinations. The d-dimensional case equations are not stated here for evident reasons. One can prove that:

$$\left|C_{x_1x_2\ldots x_d}\right| = \left|K_{x_1x_2\ldots x_d}\right| = d\left(d-1\right)+1 \tag{7}$$

Thus, $\left|K_{x_1x_2\ldots x_d}\right| = 1(mod2)$; i.e., each processor unit has an odd number of testing neighbors that makes it possible to apply the majority operator to produce the resulting faulty/non-faulty flag. According to (7), the number of testing neighbors in 2-dimensional meshes is minimal: $\left|K_{xy}\right| = 3$. In a 3-dimensional array, each unit has $\left|K_{xyz}\right| = 7$ testing neighbors.

4. THE MUTUAL INTER-UNIT TEST PROCEDURE

The process of mutual inter-unit test may be represented as a parallel algorithm including a set of threads $B_1, B_2, \ldots, B_{d(d-1)+1}$, where thread B_i defines a test statement sequence corresponding to tested neighbor $u_{x_1^i x_2^i \ldots x_d^i}$ (see Figure 2). The algorithm applies to a VLSI MP of any dimension $d \geq 2$.

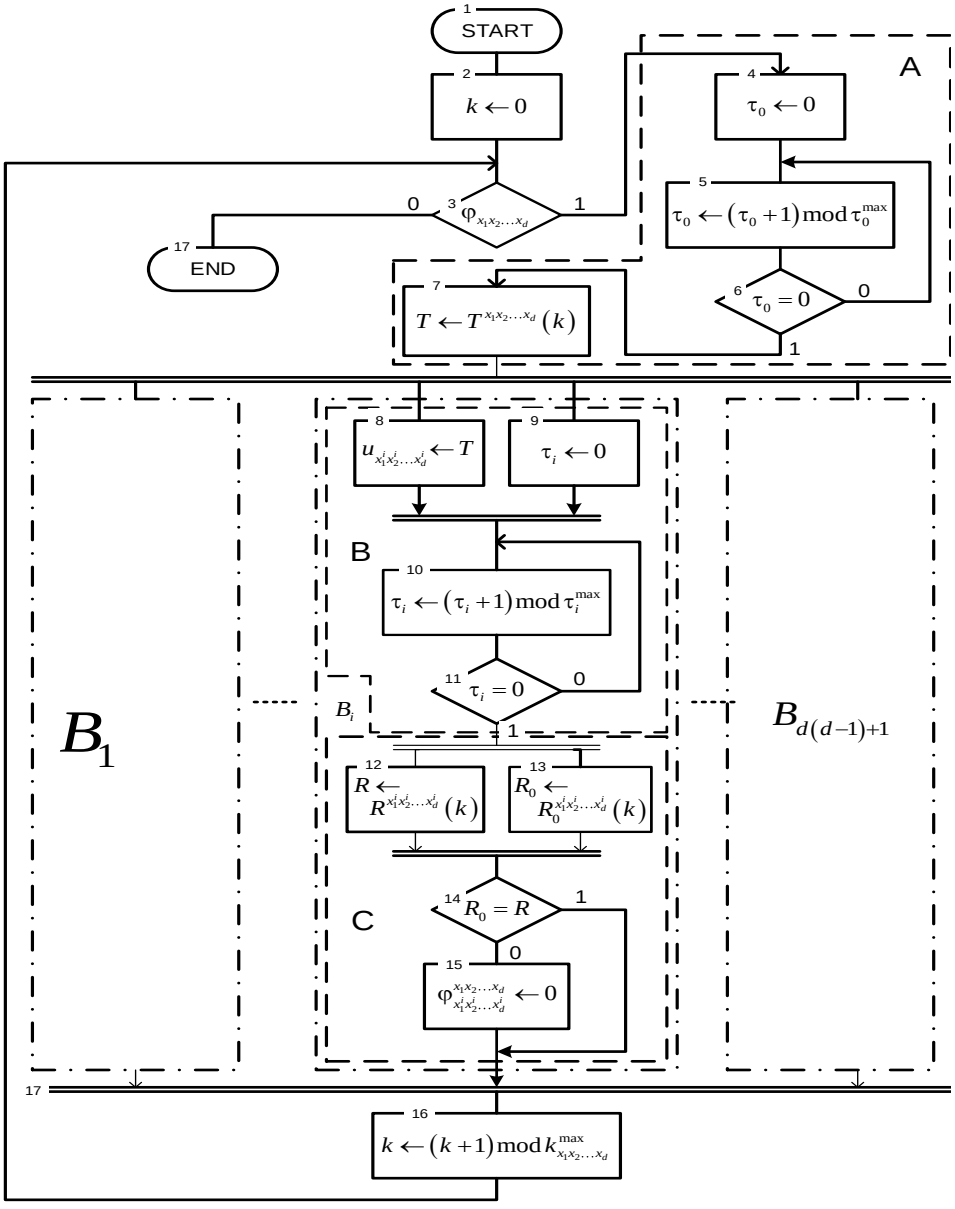

Figure 2. Flow-chart of the mutual inter-unit test algorithm.

The algorithm in Figure 2 includes the main test loop which is executed while the corresponding Processor unit (which is meant to be $u_{x_1x_2\ldots x_d}$) is considered healthy by its testing neighbors $K_{x_1x_2\ldots x_d}$ (see condition 3). As another loop begins, a new test signature $T^{x_1x_2\ldots x_d}(k)$ is formed (see statement 7), which is simultaneously transferred to tested neighbors $C_{x_1x_2\ldots x_d}=\left\{u_{x_1^ix_2^i\ldots x_d^i}\right\}$ (see statement 8). After all the tested neighbors have returned corresponding response signatures $\left\{R^{u_{x_1^ix_2^i\ldots x_d^i}}(k)\right\}$ (see statement 12), a decision is made by the processor $u_{x_1x_2\ldots x_d}$ whether a particular tested neighbor $u_{x_1^ix_2^i\ldots x_d^i}$ is faulty or healthy (see condition 14 and statement 15).

The algorithm in Figure 2 consists of three main sections: A, B and C (see the dash lines). Section A is necessary to spin τ_0^{max} clock ticks until the next test loop begins and another test signature $T^{x_1x_2\ldots x_d}(k)$ gets ready for transfer. Section B is responsible for transferring the test signature to tested unit $u_{x_1^ix_2^i\ldots x_d^i}$ and performs counting τ_i^{max} clock ticks until a response from the tested processor is supposed to arrive. Section C first controls the arrival of test response $R^{u_{x_1^ix_2^i\ldots x_d^i}}(k)$ from unit $u_{x_1^ix_2^i\ldots x_d^i}$ and then generates reference test response $R^{x_1x_2\ldots x_d}(k)$ to compare it to $R^{x_1^ix_2^i\ldots x_d^i}(k)$. If the above are equal, then tested neighbor $u_{x_1^ix_2^i\ldots x_d^i}$ is assumed to be healthy; otherwise, it is considered faulty and the partial faulty/non-faulty decision flag $\varphi_{x_1^ix_2^i\ldots x_d^i}^{x_1x_2\ldots x_d}$ is reset to zero. This flag is then used in Equations like (3) and (6) (depending on the value of d) to produce the final decision flag $\varphi_{x_1^ix_2^i\ldots x_d^i}$. The meaning of the symbols used in the flowchart of Figure 2 is presented in Table 1.

Table 1. The meaning of the symbols used in Figure 2.

Symbol	Meaning
$k_{x_1x_2\ldots x_d}^{\max}$	The number of test signatures supported by processor unit $u_{x_1x_2\ldots x_d}$
$k,\ k=\overline{0,k_{x_1x_2\ldots x_d}^{\max}-1}$	Test signature counter of processor unit $u_{x_1x_2\ldots x_d}$
$\tau_0^{\max}$	The interval (in clock ticks) between two adjacent test loops
τ_0	Next test loop wait counter
$\tau_i^{\max},\ i=\overline{1,d\left(d-1\right)+1}$	The maximum time needed to form a test response by tested processor unit $u_{x_1^ix_2^i\ldots x_d^i}$
$\tau_i,\ i=\overline{1,d\left(d-1\right)+1}$	Test response wait counter
$T^{x_1x_2\ldots x_d}\left(k\right)$	k^{th} test signature supported by processor unit $u_{x_1x_2\ldots x_d}$
$R^{x_1^ix_2^i\ldots x_d^i}\left(k\right)$	Test response signature issued by tested processor unit $u_{x_1^ix_2^i\ldots x_d^i}$ after $T^{x_1x_2\ldots x_d}\left(k\right)$ is received
$R_0^{x_1^ix_2^i\ldots x_d^i}\left(k\right)$	The reference test response signature expected to be issued by processor unit $u_{x_1^ix_2^i\ldots x_d^i}$ after receiving $T^{x_1x_2\ldots x_d}\left(k\right)$
T,R,R_0	Temporarily used variables
$\leftarrow$	The value assignment/transfer operator

In the algorithm diagrammed in Figure 2, much work is done in parallel, which makes it possible to concurrently test processor units across the entire multiprocessor structure. All the conditions and statements of the algorithm are simple enough to be implemented in hardware, which additionally contributes to the mutual inter-unit test environment performance. Yet, the test response signature mechanism used in the presented algorithm allows configuring test actions performed by tested neighbors taking into account the test complexity/duration trade-off.

5. THE MUTUAL INTER-UNIT TEST HARDWARE

The mutual inter-unit test algorithm of Figure 2 may be directly presented as a hardware-level implementation. The logic diagram of the embedded test hardware constructed according to the above algorithm is shown in Figure 3.

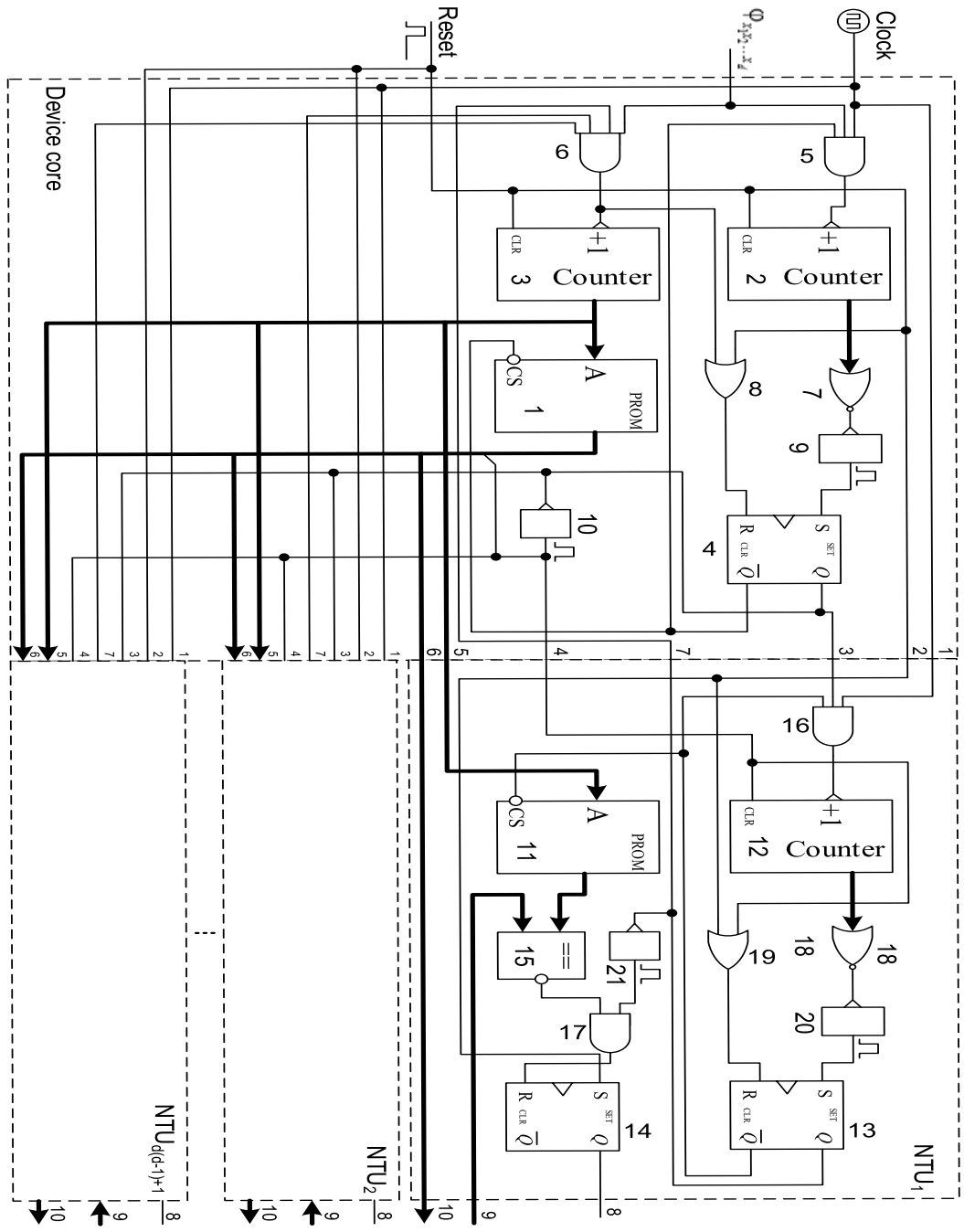

Figure 3. Logic diagram of the embedded test hardware implementing the mutual inter-unit test algorithm.

The device of Figure 3 is supposed to be a part of each processor unit; it consists of the device core and $d(d-1)+1$ neighbor test units (NTUs). The device core executes the initial and final sequential threads of the mutual inter-unit test algorithm, while NTUi implements thread $B_i, i = \overline{1, d(d-1)+1}$ (see Figure 2).Taking into account the fact that the NTUs are identical, only NTU1 is detailed in Figure 3. The adopted input/output numbering scheme helps understand the connections between the device core and the NTUs. The functions of the units and logic gates shown in Figure 3 are detailed in Table 2.

Table 2. The functions of the units and gates presented in Figure 3

Unit or gate	Function
Memory unit 1	Stores the test signatures issued by the processor unit
Circular binary counter 2	Counts the clock pulses that arrived between two adjacent test loops performed by the processor unit
Circular binary counter 3	Points to the next test signature in memory 1 to be issued by the processor unit
Flip-flop 4	Indicates whether counter 2 has zeroed or not
AND gate 5	Stops clock pulses from arriving at counter 2
AND gate 6	Stops clock pulses from arriving at counter 3
NORgate 7 together with univibrator9	Detect whether counter 2 has re-entered the zero state
OR gate 8	Necessary to OR the pulses clearing flip-flop 4
Univibrator 10	Produces a pulse which forces the NTUs to start operation
Memory unit 11	Stores the ref. response signatures for the tested neighbors of the current processor
Circular binary counter 12	Counts the clock pulses that arrived until the corresponding tested neighbor sends a response signature
Flip-flop 13	Indicates whether counter 12 has zeroed or not
Flip-flop 14	Indicates whether the corresponding tested neigh. is currently healthy or faulty
Comparator 15	Compares the test response sent by the tested neighbor to the corresponding reference test response read from memory 11
AND gate 16	Stops clock pulses from arriving at counter 12
AND gate 17	Stops reset pulses from arriving at counter 14
NOR gate 18 combined with univibrator 20	Detect whether counter 12 has re-entered the zero state
OR gate 19	Necessary to OR the pulses clearing flip-flop 13
Univibrator 21	Produces a pulse to clear flip-flop 14

6. Comparing the Mutual Inter-unit Test Approach to Self-checking

The mutual inter-unit test approach is a good alternative to the self-checking technique, providing better multiprocessor testability, which is demonstrated in the present section.

Let $\pi^+(t)$ be the probability that a processor unit of the multiprocessor is properly detected as faulty by a separate test unit (NTU). Taking into account that there are $C_j^i = \frac{j!}{i!(j-i)!}$ possible combinations of testing neighbors correctly reporting that the current processor is faulty, the following Equation may be deduced:

$$P^+(t) = \sum_{i=\left\lceil d(d-1)+1/2 \right\rceil}^{d(d-1)+1} C^i_{d(d-1)+1} \pi^+(t)^i \left[1-\pi^+(t)\right]^{d(d-1)-i+1} \quad (8)$$

Equation (8) gives the probability $P^+(t)$ that a processor unit is properly detected as faulty subject to the mutual inter-unit test approach employed.

To evaluate the effect provided by the mutual inter-unit test, we assume that $\pi^+(t)$ equals the probability of successful self-test (we presuppose that each processor has a built-in NTU or similar hardware to check its state) and then calculate $P^+(t)/\pi^+(t)$ depending on d and $\pi^+(t)$ with fixed $\pi^+(t)$ and d, respectively (see Figure 4).

(a) $P^+(t)/\pi^+(t)$ (b) $P^+(t)/\pi^+(t)$

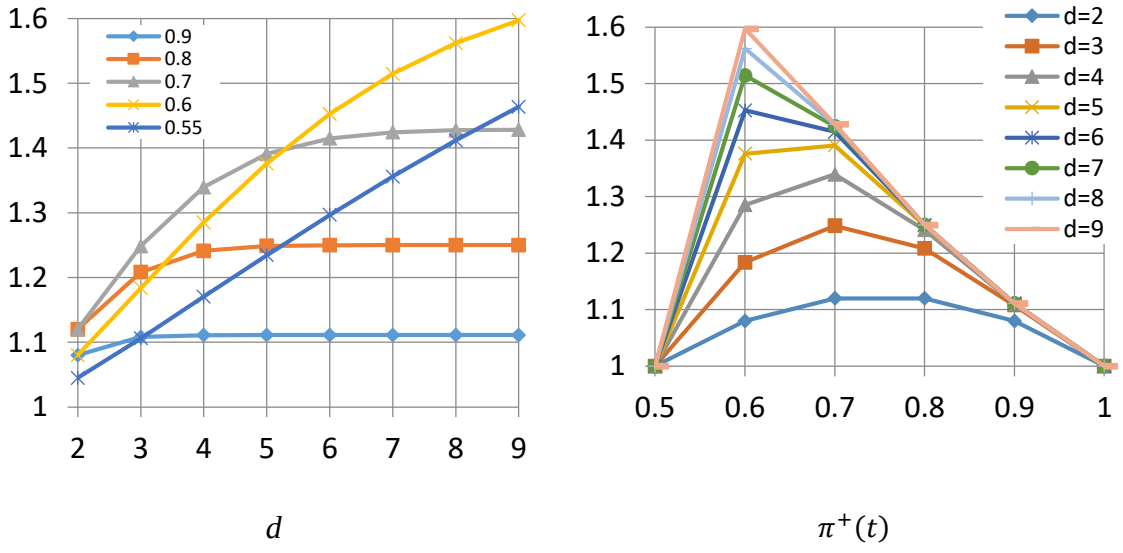

Figure 4. (a) $P^+(t)/\pi^+(t)$ versus d and (b) $P^+(t)/\pi^+(t)$ versus $\pi^+(t)$ graphs for fixed $\pi^+(t)$ and d, respectively.

The graphs in Figure 4 demonstrate that the mutual inter-unit test approach is effective as long as $\pi^+(t) \in [0.6; 0.9]$. If $\pi^+(t) \to 1$ or $\pi^+(t) \to 0.5$, then $P^+(t)/\pi^+(t) \to 1$, thus the effectiveness gracefully degrades. Our approach provides minimal effect for 2-dimensional multiprocessors (8% to 12% better than self-checking with $\pi^+(t) \in [0.6; 0.9]$). If more dimensions are added, then with $\pi^+(t) \in [0.6; 0.8]$, it is possible to get 20% or more effectiveness growth. Note that $\pi^+(t) = 0.6$ is approximately the point of maximum effectiveness as the number of dimensions increases.

7. The Area Cost of the Test Hardware

In our investigation, we have evaluated the area cost added by the test hardware. We assumed different VLSI MP dimensions d and calculated the area occupied by the logic gates in the test unit hardware. We fixed the number of test instructions supported by each processor unit k_{max}.

The graphs shown in Figure 5 demonstrate the VLSI area penalty *versus* VLSI MP dimension *d*. For low-dimension multiprocessors, the extra area remains as low as *O*(10000) logic gates, which is much lower than the area occupied by the processor core. For example, in a 3-dimensional multiprocessor, less than 18000 extra gates need to be added to each processor unit to support up to 32 test routines at each unit. If we add more test scenarios, then the VLSI area penalty will increase drastically. For example, a 3-dimensional VLSI MP needs over 260000 extra logic gates at each unit to support up to 512 different test routines.

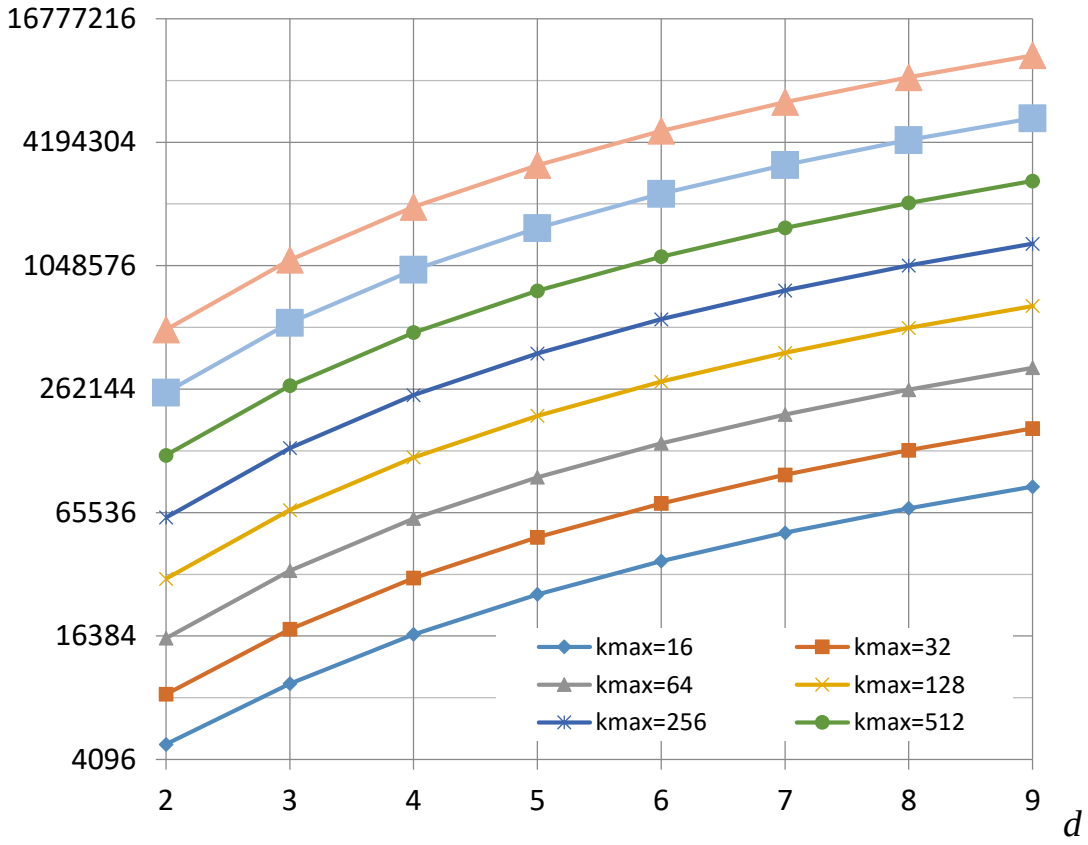

Figure 5. VLSI area (*C*) *versus d* graphs for a fixed number of test instructions supported by a particular unit (k_{max}).

As a consequence, a limited number of test instructions supported are a good option to decrease the VLSI area penalty of the test hardware. Note that each test instruction provides a specific test procedure, thus the selection of a set of test routines becomes a key issue to cover up possible fault patterns.

8. Conclusion

In the present paper, we have presented a new approach, the mutual inter-unit test mechanism, which makes it possible to improve testability of mesh-connected VLSI multiprocessors by increasing the successful fault detection probability with respect to traditional self-checking. We have shown that our approach is applicable to multiprocessors of arbitrary dimension; yet, its effectiveness grows higher as the number of dimensions increases which is important for future generation VLSI MPs. The mutual inter-unit test technique allows hardware-level testing of all the processor units across the mesh in parallel, thus significantly contributing to the test environment performance.

References

[1] Jie-qiong Chen and Guo-qiang Mao, "Capacity of Cooperative Vehicular Networks with Infrastructure Support: Multi-user Case," IEEE Trans. on Vehicular Technology, vol. 67, no. 2, pp. 1546-1560, 2018.

[2] X. D. Song and X. Wang, "Extended AODV Routing Method Based on Distributed Minimum Transmission (DMT) for WSN," Int. Jou. of Electronics and Comm., vol. 69, no. 1, pp. 371-381, 2015.

[3] S. Zhou, J. Chen and S. Liu, "New Mixed Adaptive Detection Algorithm for Moving Target with Big Data," Journal of Vibroengineering, vol. 18, no. 7, pp. 4705-4719, 2016.

[4] H. L. Niu and S. Liu, "Novel Positioning Service Computing Method for WSN," Wireless Personal Communications Journal, vol. 92, no. 4, pp. 1747-1769, 2017.

[5] Z. Ma, "A Novel Compressive Sensing Method Based on SVD Sparse Random Measurement Matrix in Wireless Sensor Network," Engineering Computations, vol. 33, no. 8, pp. 2448-2462, 2016.

[6] D. Zhang, S. Zhou and Ya-meng Tang, "A Low Duty Cycle Efficient MAC Protocol Based on Self-adaption and Predictive Strategy," Mobile Networks & Applications Jour., DOI: 10.1007/s11036-017-0878-x, 2017.

[7] S. Liu and T. Zhang, "Novel Unequal Clustering Routing Protocol Considering Energy Balancing Based on Network Partition & Distance for Mobile Education," Journal of Network and Computer Applications, vol. 88, no. 15, pp. 1-9, DOI: 10.1016/j.jnca.2017.03.025, 2017.

[8] K. Zheng and D. Zhao, "Novel Quick Start (QS) Method for Optimization of TCP," Wireless Networks, vol. 22, no. 1, pp. 211-222, 2016.

[9] D. Zhang, X. J. Kang and J. Wang, "A Novel Image De-noising Method Based on Spherical Coordinates System," EURASIP Journal on Advances in Signal Processing, no. 110, pp. 1-10, DOI: 10.1186/1687-6180-2012-110, 2012.

[10] X. Wang and X. Song, "New Clustering Routing Method Based on PECE for WSN," EURASIP Journal on Wireless Communications and Networking, no. 162, pp. 1-13, DOI: 10.1186/s13638-015-0399-x, 2015.

[11] X. Song and X. Wang, "New Agent-based Proactive Migration Method and System for Big Data Environment (BDE)," Engineering Computations, vol. 32, no. 8, pp. 2443-2466, 2015.

[12] H. L. Niu and S. Liu, "Novel PEECR-based Clustering Routing Approach," Soft Computing, vol. 21, no. 24, pp. 7313-7323, 2017.

[13] Y. Liang, "A Kind of Novel Method of Service-aware Computing for Uncertain Mobile Applications," Mathematical and Computer Modelling, vol. 57, no. 3-4, pp. 344-356, 2013.

[14] C. P. Zhao, "A New Medium Access Control Protocol Based on Perceived Data Reliability and Spatial Correlation in Wireless Sensor Network," Comp. & Elect. Engineering, vol. 38, no. 3, pp. 694-702, 2012.

[15] W. B. Li, "Novel Fusion Computing Method for Bio-Medical Image of WSN Based on Spherical Coordinate," Journal of Vibroengineering, vol. 18, no. 1, pp. 522-538, 2016.

[16] Z. Ma, "Shadow Detection of Moving Objects Based on Multisource Information in Internet of Things," Journal of Experimental & Theoretical Artificial Intelligence, vol. 29, no. 3, pp. 649-661, 2017.

[17] Z. Ma, "A Novel Compressive Sensing Method Based on SVD Sparse Random Measurement Matrix in Wireless Sensor Network," Engineering Computations, vol. 33, no. 8, pp. 2448-2462, 2016.

[18] S. Liu and T. Zhang, "Novel Unequal Clustering Routing Protocol Considering Energy Balancing Based on Network Partition & Distance for Mobile Education," Journal of Network and Computer Applications, vol. 88, no. 15, pp. 1-9, DOI: 10.1016/j.jnca.2017.03.025, 2017.

[19] G. Li and K. Zheng, "An Energy-balanced Routing Method Based on Forward-aware Factor for Wireless Sensor Network," IEEE Transactions on Industrial Informatics, vol. 10, no. 1, pp. 766-773, 2014.

[20] H. L. Niu and S. Liu, "Novel PEECR-based Clustering Routing Approach," Soft Computing, vol. 21, no. 24, pp. 7313-7323, DOI: 10.1007/s00500-016-2270-3, 2017.

[21] H. L. Niu and S. Liu, "Novel Positioning Service Computing Method for WSN," Wireless Personal Communications, vol. 92, no. 4, pp. 1747-1769, DOI: 10.1007/s11277-016-3632-y, 2017.

[22] S. Zhou, J. Chen and S. Liu, "New Mixed Adaptive Detection Algorithm for Moving Target with Big Data," Journal of Vibroengineering, vol. 18, no. 7, pp. 4705-4719, 2016.

[23] Th. Rauber and G. Runger, Parallel Programming for Multicore and Cluster Systems, Springer 2013, XIII, 516 p.

[24] Z. Wang, VLSI, InTech, 464 p, 2010.

[25] S. Furber, "Living with Failure: Lessons from Nature?," Proc. of the 11th IEEE European Test Symposium (ETS '06), pp. 4-8, May 2006.

[26] E. Kolonis, M. Nicolaidis, D. Gizopoulos, M. Psarakis, J. Collet and P. Zajac, "Enhanced Self-configurability and Yield in Multicore Grids," Proc. of the 15th IEEE Int. On-line Testing Symposium (IOLTS), pp. 75-80, Jun. 2009.

[27] G. Jiang, W. Jigang and J. Sun, "Efficient Reconfiguration Algorithm for Three-dimensional VLSI Arrays," Proc. of the 26th IEEE International Parallel and Distributed Processing Symposium Workshops & PhD Forum, pp. 261-265, 2012.

[28] W. Jigang, T. Srikanthan, G. Jiang and K. Wang, "Constructing Sub-arrays with Short Interconnects from Degradable VLSI Arrays," IEEE Transactions on Parallel and Distributed Systems, vol. 25, no. 4, pp. 929-938, April 2014.

[29] S. M. A. H. Jafri, S. J. Piestrak, O. Sentieys and S. Pillement, "Design of the Coarse-grained Reconfigurable Architecture DART with On-line Error Detection," Microprocessors and Microsystems, vol.38, no. 2, pp. 124-136, 2014.

[30] P. Bernardi, L. M .Ciganda, E. Sanchez and M. Sonza Reorda, "MIHST: A Hardware Technique for Embedded Microprocessor Functional On-line Self-Test," IEEE Transactions on Computers, vol. 63, no. 11, pp. 2760-2771, Nov. 2014.

[31] S. R. Das, "Self-testing of Core-based Embedded Systems with Built-in Hardware," IEEE Proceedings: Circuits, Devices and Systems, vol. 152, no. 5, pp. 539-546, 7 Oct. 2005.

[32] S. Lin, W. Shen, C. Hsu, C. Chao and A. Wu, "Fault-tolerant Router with Built-in Self-test/Self-diagnosis and Fault-isolation Circuits for 2-D Mesh-Based Chip Multiprocessor Systems," Proc. of the IEEE International Symposium on VLSI Design, Automation and Test (VLSI-DAT '09), pp. 72–75, Apr. 2009.

[33] C. Stroud, J. Sunwoo, S. Garimella and J. Harris, "Built-in Self-test for System-on-Chip: A Case Study," Proc. of the IEEE International Test Conf. (ITC), pp. 837-846, 2004.

[34] Z. Zhang, D. Refauvelet, A. Greiner, M. Benabdenbi and F. Pecheux, "On-the-Field Test and Configuration Infrastructure for 2-D-Mesh NoCs in Shared-Memory Many-Core Architectures," IEEE Transactions on Very Large Scale Integration (VLSI) Systems, vol. 22, no. 6, pp. 1364-1376, June 2014.

[35] R. Ahlswede and H. Aydinian, "On Diagnosability of Large Multiprocessor Networks," Discrete Applied Mathematics, vol. 156, no. 18, pp. 3464-3474, Nov. 2008.

[36] G. Miorandi, A. Celin, M. Favalli and D. Bertozzi, "A Built-in Self-testing Framework for Asynchronous Bundled-Data NoC Switches Resilient to Delay Variations," Proc. of the 10th IEEE/ACM International Symposium on Networks-on-Chip (NOCS 2016), pp.1-8, Aug. 31-Sep. 2, 2016.

[37] L. Huang, J. Wang, M. Ebrahimi, M. Daneshtalab, X. Zhang, G. Li and A. Jantsch, "Non-blocking Testing for Network-on-Chip," IEEE Transactions on Computers, vol. 13, no. 9, pp. 679 - 692, Sep. 2014.

[38] E. Cota, F. Kastensmidt, M. Cassel and M. Herve, "A High-fault Coverage Approach for the Test of Data, Control and Handshake Interconnects in Mesh Networks-on-Chip," IEEE Transactions on Computers, vol. 57, no. 9, pp. 1202-1215, 2008.

[39] J. S. Al-Azzeh, M. E. Leonov, D. E. Skopin, E. A. Titenko and I. V. Zotov, "The Organization of Built-in Hardware-Level Mutual Self-test in Mesh-Connected VLSI Multiprocessors," International Journal on Information Technology, vol.3, no. 2, pp. 29-33, 2015.

[40] J. S. Al-Azzeh, “Fault-tolerant routing in mesh-connected multicomputers based on majority-operator-produced transfer direction identifiers”, Jordan Journal of Electrical Engineering, vol.3, no. 2, pp. 102-111, 2017.

[41] J. S. Al-Azzeh, “A Distributed Multiplexed Mutual Inter-Unit in-Operation Test Method for Mesh-Connected VLSI Multiprocessors”, Jordan Journal of Electrical Engineering, vol.3, no. 3, pp. 193-207, 2017.

ملخص البحث:

يتناول هذا البحث مسألة كشف الأخطاء على مستوى المعدات في اثناء التشغيل في المعالجات المتعددة ذات التكامل على نطاقٍ واسعٍ جداً المتصلة على شكل شبكة. فقد تم تقديم طريقة جديدة لاختبار المعالجات المتعددة مبنية على الفحص المتبادل بين الوحدات؛ الأمر الذي يسمح بزيادة احتمالية الكشف الناجح عن الأخطاء. كما تم تحديد قواعد لتشكيل مجموعات فاحصة وأخرى مفحوصة من "الجيران" لكل وحدة من الوحدات، تكون ثابتة بالنسبة لموقع الوحدة ضمن البنية التركيبية للمعالج المتعدد وعدد أبعاده. وتتشكل النتيجة النهائية للاختبار لكل وحدة معالج عن طريق تطبيق عامل الأغلبية على كل واحدة من البطاقات التي تفيد بوجود خطأ أو عدم وجود خطأ والتي تم حسابها من جانب جميع الوحدات المجاورة الفاحصة.

من جهة أخرى، يعرض البحث المعادلات الخاصة بتحديد عدد الوحدات المجاورة الفاحصة لكل وحدة معالج اعتماداً على عدد أبعاد المعالج المتعدد. كذلك تم تقييم احتمالية الكشف الناجح عن الأخطاء على موثوقية وحدات الفحص منفردة. وقد أظهرت الطريقة المقترحة أنها توفر المزيد من احتمالية الكشف الناجح عن الأخطاء إذا قورنت بالاختبار الذاتي لجميع الحالات ذات الأهمية العملية.

EDITORIAL BOARD SUPPORT TEAM

LANGUAGE EDITOR

Haydar Al-Momani

EDITORIAL BOARD SECRETARY

Eyad Al-Kouz

JJCIT ADDRESS

WEBSITE: www.jjcit.org

EMAIL: jjcit@psut.edu.jo

ADDRESS: Princess Sumaya University for Technology, Khalil Saket Street, Al-Jubaiha.

B.O. BOX: 1438 Amman 11941 Jordan.

TELEPHONE: +962-6-5359949.

FAX: +962-6-7295534.

المجلة الأردنية للحاسوب و تكنولوجيا المعلومات

ISSN 2415 - 1076 (Online)
ISSN 2413 - 9351 (Print)

آب ٢٠١٨ المجلد ٤ العدد ٢

JJCIT

www.jjcit.org

jjcit@psut.edu.jo

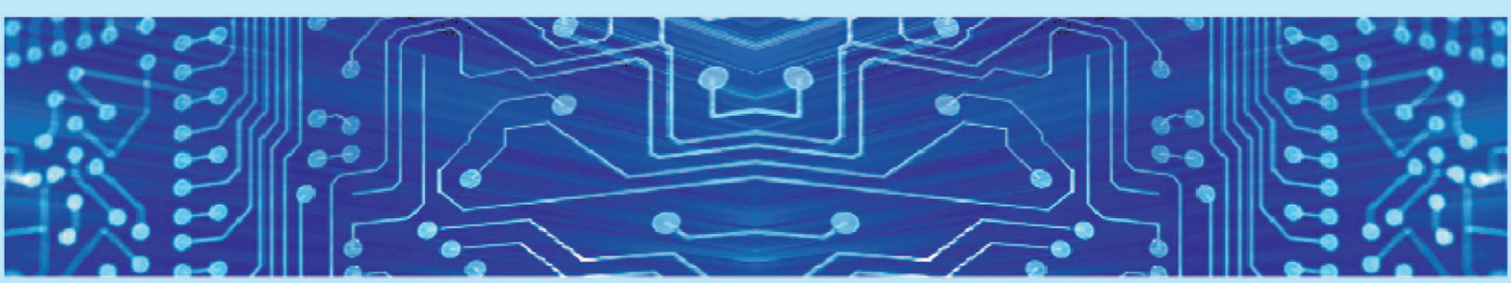

مجلة علمية عالمية متخصصة محكمة

تصدر بدعم من صندوق دعم البحث العلمي